LAWRENCE
LIVERMORE
NATIONAL
LABORATORY

LLNL-TR-659761

Pu Sorption, Desorption and Intrinsic Colloid Stability under Granitic Chemical Conditions

P. Zhao, M. Zavarin, Z. Dai, A. B. Kersting

September 4, 2014

Disclaimer

This work performed under the auspices of the U.S. Department of Energy by Lawrence Livermore National Laboratory under Contract DE-AC52-07NA27344.

August 26, 2014

Pu Sorption, Desorption and Intrinsic Colloid Stability under Granitic Chemical Conditions M4FT-14LL0807031

Pihong Zhao, Mavrik Zavarin, Zurong Dai, and Annie B. Kersting

Glenn T. Seaborg Institute, Physical & Life Sciences, Lawrence Livermore National Laboratory, 7000 East Avenue, Livermore, CA 94550, USA.

Contents

Summary

This progress report (M4FT-14LL0807031) describes research conducted at LLNL as part of the Crystalline Repository effort within the UFD program. Part I describes the dissolution kinetics of intrinsic Pu colloids synthesized in an alkaline solution. Part II describes the morphology and dissolution characteristics of various forms of Pu oxides prepared over a range of solution and temperature conditions. Proposed FY15 activities are identified.

A study of the dissolution of intrinsic Pu colloids in the presence of montmorillonite at different temperatures is summarized in Part I. Intrinsic Pu colloid prepared under alkaline conditions were found to be unstable over a timescale of months. Although these intrinsic Pu colloids tend to dissolve in the presence of montmorillonite, the subsequent formation of thermodynamically more stable Pu pseudo-colloids can play important role in Pu transport in the environment over significant temporal and spatial scales.

In Part II, we examined the reactivity of three different types of intrinsic Pu colloids in the presence of montmorillonite at 25 and 80°C under atmospheric conditions. Pu oxides calcined at 300 and 800 °C and intrinsic Pu colloids produced from acidic solution are quite stable under our experimental conditions. Only two out of seven experiments showed signs of intrinsic Pu colloid dissolution after 100 days. Predicted Pu concentrations calculated using dissolution rate constants obtained from intrinsic Pu colloids formed in alkaline solution are much higher than the measured Pu concentrations, suggesting that these three types of intrinsic Pu colloids are more stable, thus less reactive than the ones formed under alkaline conditions. The differences in the reactivity among investigated intrinsic Pu colloids are attributed to their morphological features including crystallinity, crystal growth, aggregation and particle shapes and sizes, all of which are greatly influenced by temperatures during formation of these intrinsic Pu colloids. Intrinsic Pu colloids and/or Pu oxides formed at elevated temperatures are more stable and may play an important role in the migration of intrinsic Pu colloids away from nuclear waste repository setting. Our results suggest that repository scenarios that include higher heat loading may result in stabilization of Pu oxide phases, which can lead to greater migration of intrinsic Pu colloids. However, the repository temperature history, combined with the predicted timing of canister failure and re-saturation of the repository near field will all play a role in the evolution of any specific repository scenario and the potential for Pu mobilization.

With respect to FY15 activities, we propose three taks: 1) Stability of Intrinsic Pu Colloids Across a Range of Repository Conditions, 2) Temperature Effects on Bentonite Alteration and Sorption of Actinides, and 3) Modeling Colloid Facilitated Pu Transport at the Grimsel CFM Facility.

1) We will investigate the stability of both low temperature and high fired intrinsic Pu oxides across a wide range of ionic strengths, solution conditions, and temperature that brackets a wider range of repository conditions. Particular focus will be placed on the stabilization of Pu clusters in solution at higher ionic strengths, as observed by Soderholm et al. (2008).

2) We will seek to constrain the effects of temperature on the adsorption/desorption of Pu(IV) and Pu(V) with montmorillonite and its alteration products. This effort will build on our existing experience with Pu and montmorillonite at both ambient and elevated temperatures.(Begg et al., 2013a; Zhao et al., 2012) We will take advantage of the availability of large-volume titanium Parr bomb reactors at LLNL to prepare hydrothermally altered montmorillonite and bentonite rock (6 months alteration at 200ºC). The

sorption/desorption of Pu(IV) and Pu(V) to both pristine and hydrothermally altered rock will be investigated as a function of pH (4-10) and temperature (25-80ºC).

3) Recently, we have developed a numerical model to describe the adsorption and desorption behavior of Pu with montmorillonite (a primary constituent of bentonite) colloids.(Begg et al., In Prep) To further test the assumptions in our approach, we propose to apply this numerical model to data generated in recent Pu-colloid transport experiments performed at the Grimsel Test Site. Comparison of the model and observed behavior will allow us to verify the applicability of our in field-scale conditions or will otherwise highlight areas of weakness in our understanding of Pu adsorption/desorption mechanisms.

Part I: New Insights into the Stability of Plutonium Intrinsic Colloids in the Presence of Clay at Elevated Temperatures: Dissolution Kinetics

1. Introduction

The large volumes of plutonium (Pu) designated for storage in high-level nuclear waste repositories are predicted to impact repository performance under certain scenarios (Kaszuba and Runde, 1999; Management, 2002). Plutonium can migrate in the subsurface associated with the colloidal fraction of groundwater (Kersting et al., 2012). Colloid facilitated Pu transport has been reported on the scale of kilometers at sites both in the US (Kersting et al., 1999; Santschi et al., 2002b) and Russia (Novikov et al., 2006). Despite the recognized importance of colloid-facilitated Pu transport, geochemical and biochemical mechanisms controlling Pu colloid formation and stability over the range of concentrations expected in the environment have not been identified. In particular, kinetic information under environmental conditions is lacking. The temperature in the vicinity of radiological waste packages is expected to be elevated for some time. Thus, understanding Pu behavior at elevated temperatures is necessary. The paucity of thermodynamic and kinetic data limits the efficacy of current transport model predictions (Altmaier et al., 2013; Rao et al., 2011).

Pu can be associated with the colloidal fraction of groundwater in two forms. Pu can either form an intrinsic colloid or sorb onto mineral, organic, or microbial colloids to form pseudo-colloids. At high concentrations where actinide ions in solution exceed the solubility product, Pu will precipitate and form Pu hydroxide intrinsic colloids (Neck et al., 2007d; Neck and Kim, 2001). Transport of intrinsic Pu colloids is controlled by its stability (both physical and chemical). At low concentrations, Pu will sorb onto inorganic or organic colloids, resulting in the formation of pseudo-colloids. Transport of Pu pseudo-colloids is determined by the Pu sorption/desorption kinetics. Both forms of Pu colloids may exist simultaneously under some subsurface conditions.

The identity of naturally occurring mineral colloids will be a function of the host rock mineralogy. Among the most ubiquitous mineral colloids are aluminosilicate clays that are commonly observed as mobile colloids due to their inherently small particle size and prevalence as alteration minerals from original host rock material (Kersting et al., 1999). Clays are known to sorb Pu (Begg et al., 2013b; Bertetti et al., 1998; Keeney-Kennicutt and Morse, 1985; Kozai et al., 1996; Kozai et al., 1993; Lujaniene et al., 2007; Powell et al., 2004; Powell et al., 2005; Powell et al., 2008; Sabodina et al., 2006b; Sanchez et al., 1985; Turner et al., 1998). In addition, the proposed use of bentonite within some engineered barrier systems scenarios for high-level nuclear waste repositories provides additional importance to understanding Pu interaction with smectite aluminosilicate clays (Sabodina et al., 2006b). Smectite clay may represent a key phase that will control transport of Pu pseudo-colloids in repository near and far fields.

Batch sorption has been the most common method used to measure the affinity of a contaminant for a mineral surface. Data obtained from a conventional sorption experiment are the concentrations of the contaminant in the liquid phase before and after sorption. Filtration and/or centrifugation are commonly used to separate solids from liquid after equilibrium is reached. The quantity sorbed is calculated based on the difference of the total and aqueous concentrations. However, if the contaminant is involved in multiple processes that all form solid phases (i.e., sorption, colloids formation and/or precipitation), these data cannot distinguish between them.

In order to distinguish between precipitated, colloidal, and sorbed states of Pu, we employed dialysis membranes to segregate Pu intrinsic colloids from pseudo colloids in the current study. Dialysis membranes are commonly used to separate suspended solutes or particles of different

dimensions in a liquid mixture. Desirable size separation by dialysis can be achieved by selecting the membrane pore-size molecular weight cutoff (MWCO). A membrane pore size of 5 kilo Daltons (kDa) is able to separate soluble species from particles >1 nm. Dialysis membranes provide a unique opportunity to segregate Pu intrinsic colloids (2−5 nm) from its pseudo-colloids (>100-nm on mineral phases) while allowing aqueous species (<1 nm) to interact with both colloidal phases.

In the present study, we examined the stability of Pu intrinsic colloids relative to Pu-montmorillonite pseudo-colloids using a novel experimental design and modeling approaches. We employed dialysis membranes in an effort to segregate Pu intrinsic colloids (2−5 nm) from montmorillonite colloids (>100 nm) and allow aqueous Pu to establish equilibrium between both colloidal phases. Using the dialysis membrane approach, we monitored the dissolution of PuO_2 intrinsic colloids in the absence and presence of montmorillonite, and formation of Pu pseudo-colloids. The data provide new insights into stability of plutonium intrinsic colloids in the presence of clay at 25 and 80 °C.

2. Materials and Methods

2.1 Pu Stock and Intrinsic Pu colloid preparation

All reagents were of analytical grade or better and used as received. De-ionized water from a Barnstead Milli‑Q Water (MQW) purification system (resistivity: 18.2 megaohm-cm) was used for all procedures and solution preparation. Pu stock solutions with two different Pu isotopic ratios were used. A relatively pure alpha-emitting ^{238}Pu stock solution was used in low- and intermediate Pu concentration experiments. The ^{238}Pu, ^{239}Pu, ^{240}Pu, and ^{241}Pu mass percent in the stock was 76.83%, 21.03%, 2.01%, and 0.142%, respectively. The major isotope contributing to alpha activity in this stock was ^{238}Pu (~99.9% by activity). The second Pu stock solution, used in the high Pu concentration experiments, was a ^{242}Pu solution spiked with ~1% of the ^{238}Pu stock. The ^{238}Pu, ^{239}Pu, ^{240}Pu, ^{241}Pu, and ^{242}Pu mass percent in this stock was 0.75%, 0.21%, 0.13%, 0.04%, and 98.87%, respectively. The major isotopes contributing to alpha activity in this stock were ^{238}Pu (96.75%) and ^{242}Pu (2.93%). Both Pu stock solutions were purified using AG®1-x8 100-200 mesh anion exchange resin from Bio-Rad Laboratories, and filtered through an Amicon Ultra 0.5 mL centrifugal filter with membrane MWCO of 3 kDa from EMD Millipore. The oxidation state of Pu(IV) was confirmed using both UV-Vis and solvent extraction. The aqueous Pu(IV) starting solution was prepared by diluting the stock solution into a pH 8 buffer solution and gradually adding microliters of NaOH (1 N or 6 N) to adjust pH to ~pH 8. The intrinsic PuO_2 colloids were prepared by neutralizing Pu(IV) stocks using NaOH solution and adjusting solution pH to 9 to 10. After aging for more than a week, the Pu colloids were centrifuged at an RCF of 9168 for 1 hr, and the supernatant was removed. The Pu colloid particle size cut-off based on centrifugation was 14 nm. However, the average particle size of the aggregates (intrinsic Pu nano-colloids) was 30 nm and the sizes of crystallite within the aggregates ranged from 2.5 to 4.5 nm (Figure 1). The Pu colloids were re-suspended in Milli-Q water. The Pu colloid starting solutions were prepared by adding a spike of Pu colloids into the pH 8 buffer solution without further pH adjustment. Pu concentrations in samples were analyzed by a PerkinElmer Tri-Carb 2900TR Liquid Scintillation Analyzer. The fraction of soluble Pu in the Pu colloid stock solution, based on the 3 kDa MWCO filtrate, was 1 to 3%.

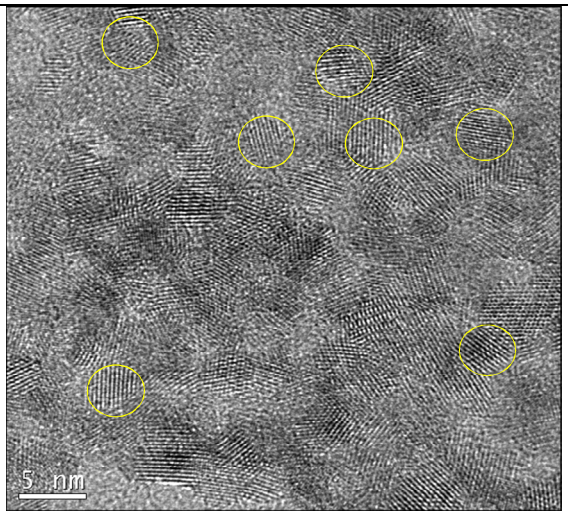

Fig. 1. TEM image of mat of Pu intrinsic colloids. Several individual Pu colloids are highlighted by yellow circles. The measured average particle sizes was 3.5 nm with a range of 2.5-4.5 nm.

2.2 Montmorillonite

SWy-1 montmorillonite (Clay Minerals Society) was pre-treated using 1 mM HCl (to dissolve any carbonate minerals) followed by addition of 0.1% H_2O_2 (to oxidize organic contaminants and reduced metals (e.g., Fe^{2+}). The pre-treated montmorillonite was centrifuged to remove excess liquid, and the wet paste was transferred to a 6 to 8 kDa MWCO dialysis tube suspended in 0.01 M NaCl solution to produce a homoionic Na-montmorillonite. The clay minerals were dialyzed for seven days, and the NaCl solution was changed at least once per day. The clay minerals were then suspended in Milli-Q water and centrifuged to obtain the fraction of particle sizes from 50 nm to 2 microns. The wet solids were dried at 40 $^{\circ}$C until a constant weight was obtained. A stock montmorillonite suspension was made by mixing 4 g of dried montmorillonite in 400 mL of pH 8 buffer (5 mM NaCl/0.7 mM $NaHCO_3$). Quadrasorb SI surface area and pore size analyzer from QuantaChrome Instruments was used for BET measurements. The surface area of montmorillonite measured by N_2(g)-BET was 31.45 ± 0.17 m^2/g, which is comparable to the reported value of 31.8 m^2/ g (Clay Minerals Repository).

2.3 Dissolution Experiments

Intrinsic Pu(IV) colloid stability was evaluated using the experimental design shown in Figure 2. Briefly, intrinsic Pu colloids are placed inside the dialysis bag, while the clay colloids are placed outside the dialysis bag. Thus, the colloidal montmorillonite is isolated from the intrinsic Pu colloids while exchange of truly aqueous (non-colloidal) ions between both solid phases is permitted. Pu detected outside the dialysis membrane over time represents dissolved Pu species that diffuse across the dialysis membrane. In the presence of montmorillonite, the dissolved Pu can either remain in solution or sorb to montmorillonite. The dissolution rate of intrinsic Pu colloids is expected to be a function of its solubility, surface area, composition, solution ionic strength, pH and temperature. The sorption rate of Pu to montmorillonite is affected by the Pu speciation, solution Eh/pH, ionic strength, and temperature.

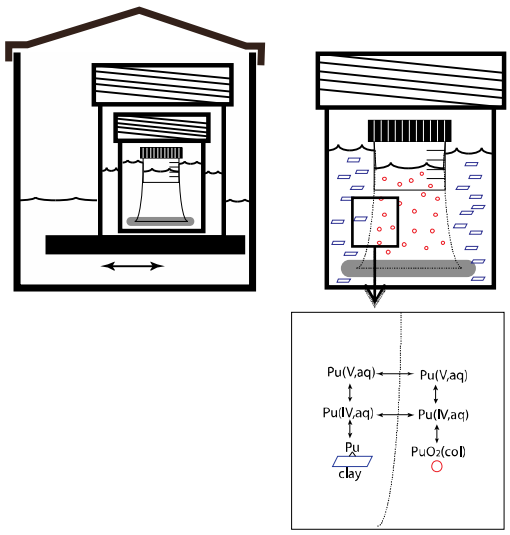

Fig. 2. Experimental design using dialysis membrane to separate intrinsic Pu colloids (placed inside dialysis tubing), from mineral colloids (placed outside the tubing). For Pu-montmorillonite sorption to occur, Pu intrinsic colloids must dissolve and diffuse through the membrane.

A total of 16 experiments (excluding a control blank) were performed to test the experimental design and quantify dissolution of intrinsic Pu colloids in the presence of montmorillonite (Table 1). The dialysis membrane used was Spectra/Por® 7 standard RC pre-treated dialysis tubing with MWCO 1 kDa, from Spectrum Laboratories, Inc. The experiments were performed at two temperatures, 25°C (8 experiments) and 80°C (8 experiments) to evaluate the effect of temperature. At each temperature, Pu was initially added either in an aqueous form (to test simple diffusion and sorption of Pu) or as intrinsic colloids (to test intrinsic colloid dissolution, diffusion and sorption of Pu). The initial Pu concentrations bracketed the PuO_2(am, hyd) solubility (~5×10^{-9} M) (Neck et al., 2007c). In addition, montmorillonite-free solutions (spiked blanks) with initial Pu concentrations below and near PuO_2(am, hyd) solubility were used to compare with sorption experiments and evaluate Pu loss to container walls and dialysis membranes.

Table 1. Experimental conditions and data summary

Exp	Temperature	Inside dialysis bag				Outside dialysis bag		Kinetic constant						Equilibrium constant
		Pu colloids	Pu^{4+}	PuO_2^+	^3H	Clay [a]	Final % Pu	k_1	k_2	k	k_3	k_{-3}	$k_s=k_1/SSA$	$K = k_3/k_{-3}$
	°C	---------- mol L^{-1} ----------				g L^{-1}		---------- day^{-1} ----------					mol m^{-2} day^{-1}	
1	25	1.13E-11				1	45	0.025					6.2E-07	
2		9.09E-10				1	33	0.06					1.5E-06	
3		2.01E-07				1	10	0.4					9.9E-06	
4		9.13E-10				0	2			0.06	0.8	0.005		160
5	80	1.14E-11				1	88	0.17					4.2E-06	
6		8.31E-10				1	70	0.3					7.4E-06	
7		2.01E-07				1	15	0.15					3.7E-06	
8		9.13E-10				0	35			0.3	20	0.8		25
9	25		5.93E-12			1	55		30					
10			6.20E-10			1	37		30					
11			6.52E-12			0	3			30	0.14	0.005		28
12	80		5.93E-12			1	100	0.15					3.7E-06	
13			6.20E-10			1	63	0.2					5.0E-06	
14			6.52E-12			0	28			0.3	0.002	0.03		0.007
15	25			1.30E-10	4.90E-11	0	89/98 [b]		25/40 [b]					
16	80			1.30E-10	4.70E-11	0	42/87 [b]		30/40 [b]					

a. Swy-1 Montmorillonite
b. values represent as $PuO_2^+/^3H$

All batch experiments were conducted in 450-mL Teflon jars with air-tight closures. 225 mL of pH 8 buffer (5 mM NaCl / 0.7 mM $NaHCO_3$) was mixed with 25 mL of montmorillonite stock suspension to yield a 250-mL montmorillonite suspension of 1 g/L. A sealed dialysis tubing containing 30 mL of either aqueous Pu(IV) or intrinsic Pu colloids was then placed in the 250 mL pH buffer solution with or without montmorillonite. The 450-mL Teflon jars were submerged in 1-L Teflon containers filled with Milli-Q water to minimize evaporative losses and provide secondary containment to the radioactive samples. Over the course of the experiment, the 25°C samples were placed on a top-loading orbital shaker, and the 80°C samples were submerged in an Innova 3100 water bath shaker from New Brunswick Scientific. All samples were shaken at an orbital speed of 100 rpm.

Each experiment was sampled as a function of time over a three-month period. At each sampling interval, aliquots of the montmorillonite suspension were collected, centrifuged and analyzed for total Pu, Pu in the supernatant, and solution pH. Alternatively, aqueous Pu was determined by measuring the filtrate Pu concentration after filtering the suspension through 3kDa pore size centrifugal filters. The montmorillonite concentration in the suspension was also measured based on light scattering at a wavelength range of 300−500 nm using a Cary 500 Scan UV-Vis-NIR spectrophotometer (Varian). The pH of the clay suspension was monitored and maintained at pH 8 ± 0.5 at all times.

3. Results and Discussion

3.1 Kinetics

The formation of Pu-montmorillonite pseudo-colloids due to the dissolution of intrinsic Pu colloids in the system involves a series of processes including Pu colloids dissolution, Pu(IV)/Pu(V) redox reactions, aqueous Pu species diffusion and sorption. To simplify the discussion, we focus on the essential processes, which follow a sequential order: PuO_2 colloids dissolve to produce aqueous Pu species inside the dialysis membrane (Eq. 1); the aqueous Pu species diffuse across the membrane (Eq. 2) and Pu species sorb onto clay that is placed outside of the dialysis membrane (Eq. 3).

$$PuO_2(s)\,|\,inside \xrightarrow{k_1} Pu(aq)\,|\,inside \quad (1)$$

$$Pu(aq)\,|\,inside \xrightarrow{k_2} Pu(aq)\,|\,outside \quad (2)$$

$$Pu(aq) + clay\,|\,outside \xleftrightarrow{K,\,k_3,k_{-3}} Pu-clay\,|\,outside \quad (3)$$

where k_1 and k_2 represent apparent kinetic constants of eq. 1 and eq. 2, respectively. $K = k_3/k_{-3}$ is the sorption equilibrium constant and k_3 and k_{-3} are the sorption and desorption rate constants.

To a first order approximation, we assume that the rates are proportional to the reactant concentrations in above equations. Therefore, a pseudo 1st order reaction model was used for all three reactions. As a result, kinetic rate constants can be compared directly to determine the rate limiting steps. However, it should be noted that k_1 is a product of intrinsic Pu colloids' specific surface area and dissolution rate constant. Similarly, k_2 reflects the characteristics of an ion's diffusion coefficient but is also a function of experimental parameters, including the configuration/dimensions of the dialysis systems, the number of membrane pores and their sizes, and shaker speed used in the experiments. By placing either aqueous or solid Pu species inside

dialysis bag, and analyzing the total Pu concentration outside of dialysis bag, we are able to determine k_1 and k_2. By analyzing concentrations of total and aqueous Pu in clay suspension outside of the bag, we can obtain equilibrium constant K.

3.2 Apparent Diffusion in the System

To determine the rate of aqueous species diffusion from inside the dialysis bag, through the membrane, and to the outside of the dialysis bag, tritium and aqueous Pu(V) were placed inside the dialysis bag and small aliquots of the solution outside dialysis bag were taken as function time and monitored for both Pu and tritium (i.e. Eq. 2). The concentrations of ^3H or PuO_2^+(aq) inside and outside of dialysis bag can be described by the following:

$$\frac{dC_{in}}{dt} = -k_2 C_{in} \quad (4)$$

$$C_{out}V_{out} = C^0(V_{in} + V_{out}) - C_{in}V_{in} \quad (5)$$

$$C^0 = C_{in}^0 * V_{in} / (V_{in} + V_{out}) \quad (6)$$

$$C_{out} = C^0[1 - \exp(-k_2 t)] \quad (7)$$

where C_{in} and C_{out} are ^3H or PuO_2^+ concentrations (in mol L^{-1}) inside and outside of the dialysis bag at time t (days), respectively; C_{in}^0 is the initial concentration inside a dialysis bag at time zero. V_{in} and V_{out} (in L) are the solution volumes inside and outside of dialysis bag, respectively.

The data obtained from diffusion experiments are plotted in Fig. 3, which shows that tritium data obtained from both temperatures (Fig. 3a) and PuO_2^+ data obtained from 25 °C (dash line in Fig. 3b) experiments fit well to a 1st order reaction model. The obtained rate constants were 40 and 23 day^{-1} for tritium at both temperatures and PuO_2^+ at 25 °C, respectively. The 1st order reaction model only fits the initial data points of PuO_2^+ at 80 °C with a rate constant of 30 day^{-1}. As time progresses, Pu concentrations at 80 °C decreased. The decrease may reflect slow sorption to container walls, sorption to the dialysis membrane, and/or oxidation/reduction of Pu(V). This data could be fit with a first order reaction followed by kinetically controlled sorption process (eq. 2 and eq. 3) (Fig. 3b). All fitted rate constants are listed in Table 1. The fitted rate constants indicate that diffusion of aqueous species across the dialysis membrane will occur on timescale of <<1 day.

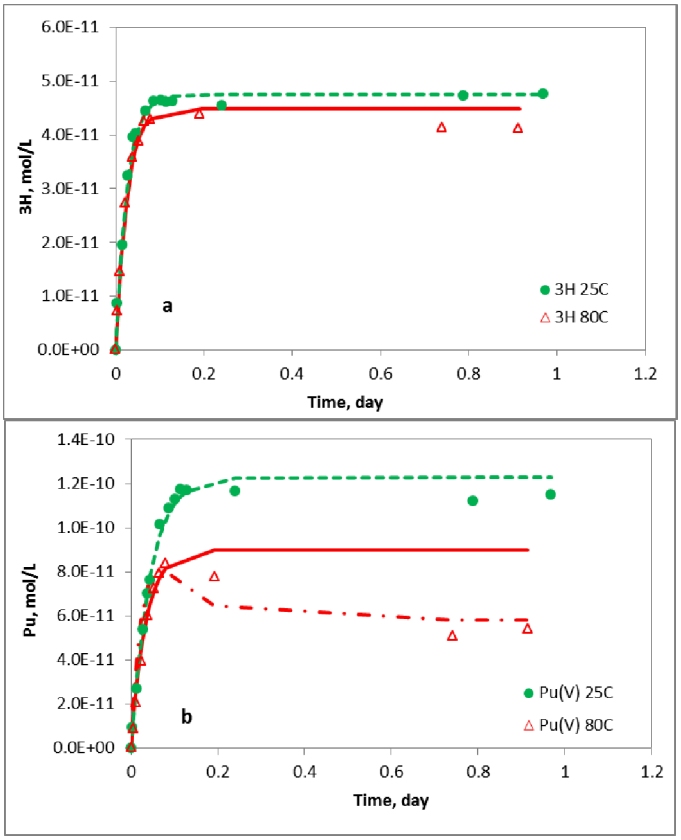

Fig. 3. Diffusion of (a) ^{3}H and (b) Pu(V) as function of time (Solid circles=25°C and open triangles=80 °C). Dash (25 °C) and solid lines (80 °C) are fitted curves using Equation 7. The dash-dotted line (PuO2+ at 80 C) is fitted by including a kinetic sorption process..

3.3 Kinetics of Intrinsic Pu Colloid Dissolution

In these experiments (Exp. 1-3, 5-7 in Table 1), intrinsic Pu colloids were placed inside the dialysis bag, which was suspended in a clay suspension. Small aliquots of the clay suspension outside dialysis bag were taken as function of time and concentrations of total and aqueous Pu was monitored. If the total Pu concentration in the clay suspension is used to evaluate the system, then the system can be simplified to containing only two processes (dissolution and diffusion). Assuming 1st order rates for Pu colloid dissolution and diffusion, the kinetics can be described by two first order reactions in sequence (Lasaga, 1998a):

(8)

where C_{out} in mol L^{-1} represents the total Pu concentration in the clay suspension as a function of time (t), and k_1 and k_2 are first order rate constants representing dissolution and diffusion. In the case where rate constants k_1 and k_2 differ by orders of magnitude, the rate-limiting process can be identified and the model can be further simplified to a first order rate model. Equations 7 and 8 provided equivalent quality of fits to the data and suggests that the dissolution process is the rate-limiting step. The rate constants ranged from 0.025-0.40 day^{-1} at 25 °C and 0.15-0.30 day^{-1} at 80

°C, one to two orders of magnitude lower than the rate constants determined in the diffusion experiments. The experimental data are plotted in Fig. 4 and the rate constants are summarized in Table 1. Dissolution of minerals with low solubility is more likely to be controlled by reactions at sites on the surface rather than material transport, either in aqueous solution or through protective surface layers (Berner, 1981). As PuO_2 is a low solubility solid phase, our results are consistent with this interpretation.

Our results also show that the dissolution rates vary with the initial Pu colloids concentration and temperature. We will discuss temperature effects in a later section. In a heterogeneous system and at constant pressure and temperature, the overall dissolution rate of a metal oxide can be described as the sum of the rates of proton-promoted, hydroxide-promoted, ligand-promoted and reductant or oxidant-promoted, if any redox reaction involves in the dissolution. In other words, the dissolution rate is actually the sum of all the parallel dissolution rates of different metal centers (Stumm, 1997). We cannot distinguish between these processes here. However, the dissolution rate clearly increases with the intrinsic Pu colloid concentration, as would be expected for a surface-controlled dissolution process.

In the high colloid concentration samples, the overall rate may decrease significantly as the system reaches equilibrium (Lasaga, 1981; Lasaga and Luttge, 2004). The impact of solution saturation can explain the decrease in kinetic constant obtained in the highest Pu concentration experiment at 80 °C (Experiment 7, Table 1). The result also implies that the solubility of Pu colloids may be lower at elevated temperatures.

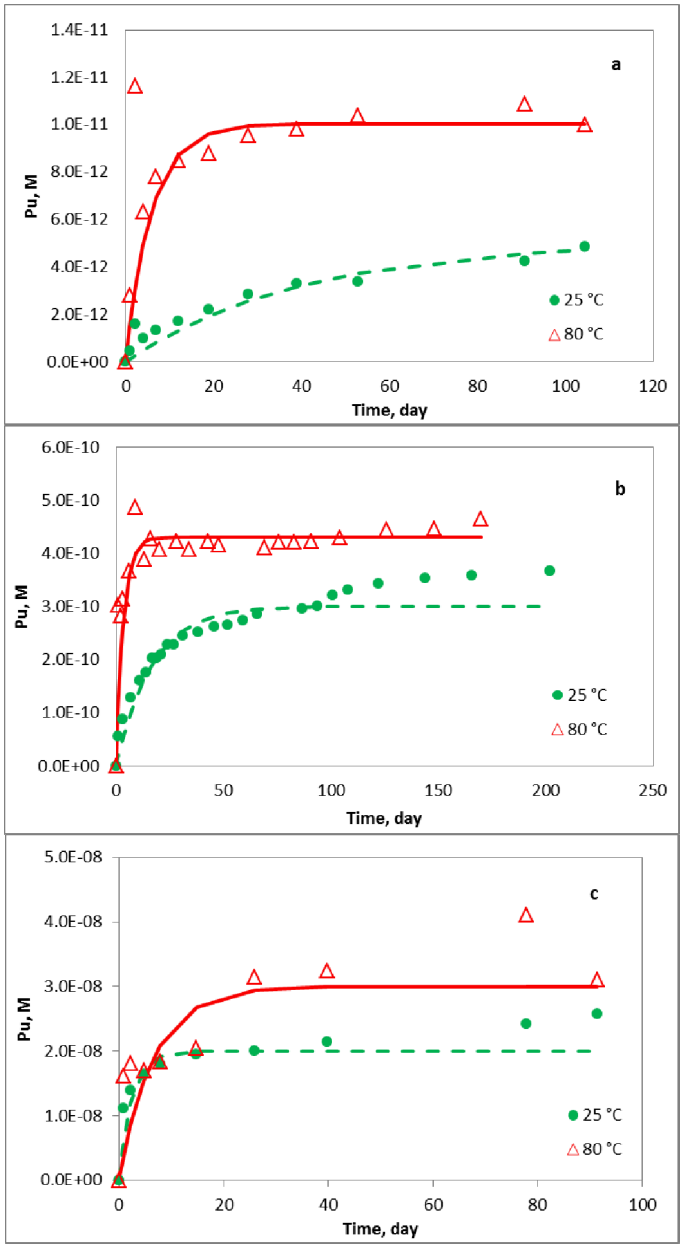

Fig. 4. Dissolution and diffusion of Pu colloids in the presence of clay at 25 and 80 °C. Solid circles (25°C) and open triangles (80 °C) are the experimental data points. Dash (25 °C) and solid lines (80 °C) are fitted curves using psuedo1st order reaction model. Initial Pu colloids concentrations were 4a: $1.1x10^{-11}$ mol L^{-1}; 4b: $9x10^{-10}$ mol L^{-1}; 4c: $2x10^{-7}$ mol L^{-1}

3.4 Sorption Kinetics in the Aqueous Pu(IV)-Montmorillonite System

Four experiments (Exp. 9, 10, 12, 13) were performed using aqueous Pu(IV) instead ofintrinsic Pu colloids. The purpose of these experiments was to investigate Pu speciation effects on the kinetics. The experimental data are plotted along with fitting curves in Fig. 5 and the obtained rates constants are listed in Table 1. The fast rates (30 day^{-1}) observed at 25 °C suggest that these

experiments were diffusion controlled and that the rate of aqueous Pu(IV) sorption to montmorillonite was much faster (Begg et al., 2013b). However, the rate constants obtained from the 80 °C experiments (Exp. 12 and 13) were much lower (0.15-0.2 day^{-1}) and similar to those obtained from intrinsic Pu colloid-montmorillonite experiments. In fact, these rate constants are 200X slower than the ones observed at 25 °C. This observation suggested that aqueous Pu(IV) species formed intrinsic Pu colloids or PuO_2 solids at 80 °C at the start of the experiment. Once these intrinisc Pu colloids formed inside the dialysis bag, they slowly dissolved and diffused across the membrane. Thus, at 80 °C, aqueous Pu(IV) initially formed intrinsic Pu colloids which then slowly dissolved, and aqueous Pu species diffused, and formed stable Pu-clay pseudo-colloids. Hydrolysis of Pu(IV) is endothermic and, as a result, high temperatures will favor the formation of intrinsic Pu colloids (Cleveland, 1979). In addition, the ionization constant of water, K_w, increases with temperature which can lead to a 30X increase in hydroxide concentration at pH 8 between 25 and 80 °C. This will also enhance Pu^{4+} hydrolysis. Endothermic hydrolysis behavior of aqueous Pu and other actinide species has been reported in numerous studies (Altmaier et al., 2013; Rao et al., 2004; Rao et al., 2011; Runde et al., 2002).

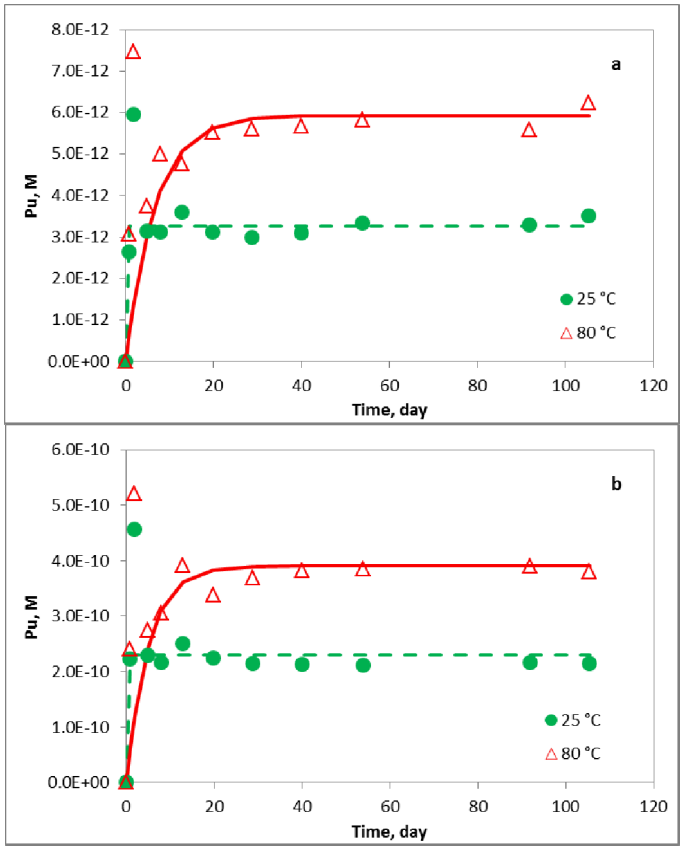

Fig. 5. Kinetics of aqueous Pu(IV)-montmorillonite system at temperatures 25 and 80 °C. Solid circles (25°C) and open triangles (80 °C) are the experimental data points. Dash (25 °C) and solid lines (80 °C) are fitted curves using 1st order kinetic model. Initial Pu colloids concentrations 5a: $6x10^{-12}$ mol L^{-1}, 5b: $6.2x10^{-10}$ mol L^{-1}.

3.5 Kinetics in the Absence of Montmorillonite

Four experiments (exp. 4, 8, 11, 14) using both intrinsic Pu colloids and aqueous Pu(IV) as were performed in the absence of a montmorillonite clay suspension. These experiments served as control experiments to evaluate the sorption of Pu to the container walls, dialysis membrane and other materials. The experimental data are plotted along with fitting curves in Fig. 6. At 25 °C, Pu concentrations in the solution outside of the dialysis bag were initially higher than at 80 °C, and then decreased over time, indicating there was significant sorption to the dialysis bag and/or container wall over time. To first order, the processes in this system can be described as a 1st order reaction followed by a sorption reaction:

$$Pu \mid inside\ bag \xrightarrow{k} Pu \mid \text{outside bag} \qquad (9)$$

$$Pu + membrane \xleftrightarrow{K,\, k_3, k_{-3}} Pu * membrane \qquad (10)$$

The Pu concentration outside of the dialysis bag as a function of time is governed by Equation 11:

$$C_{out} = C^0 \left[1 - \exp(-kt) - \frac{k_3}{k_3+k_{-3}} \left(1 + \frac{k*\exp(-(k_3+k_{-3})t) - (k_3+k_{-3})\exp(-kt)}{k_3+k_{-3}-k}\right)\right] \qquad (11)$$

where k represents kinetic constant of either PuO_2 dissolution or aqueous Pu(aq) diffusion across the membrane; $K = k_3/k_{-3}$ is sorption equilibrium constant, and k_3 and k_{-3} are the sorption and desorption rate constants.

Table 1 lists the curve fitting results and shows that rate constants are consistent with the ones obtained from dissolution or diffusion experiments depending upon Pu initial speciation and experimental temperatures. In the intrinsic Pu colloid –buffer solution system (exp. 4 and 8), rate constants were 0.06 and 0.3 day^{-1} for experiments performed at 25 and 80 °C, respectively. These values match k_1 values obtained in the intrinsic Pu colloid – montmorillonite experiments (exp. 2 and 6), indicating that kinetics in the intrinsic Pu colloid - buffer solution system was governed by the PuO_2 dissolution. In the aqueous Pu(IV)-buffer solution system (exp. 11 and 14), the rates constants were 30 and 0.3 day^{-1} in the 25 and 80 °C experiments, respectively. The 30 day^{-1} rate constant matches aqueous Pu(IV) diffusion rate constants obtained from Exp. 9 and 10, indicating that the diffusion process was controlling the system. Thus, we can conclude that the presence of clay impacts neither diffusion rates of Pu species nor dissolution rates of intrinsic Pu colloids. At elevated temperature, the 0.3 day^{-1} rate constant matches those obtained from intrinsic Pu colloid dissolutions experiments with or without clay (Exp. 6 and 8), suggesting that aqueous Pu(IV) underwent fast hydrolysis to form intrinsic Pu colloids, whose dissolution became a rate-limiting step governing the observed kinetics. Although the presence of clay doesn't affect the kinetics of these systems, it stabilizes Pu and increased total amount of Pu in the solution phase (see Table 1 for column of %Pu in solution phase outside of dialysis bag to compare exp. 2 with 4, exp. 6 with 8, exp. 9 with 11 and exp. 12 with 14).

Our results show that there is moderate sorption for Pu to the container walls and dialysis membrane and the sorption equilibrium constant, K, ranges from 0.067 at 80 °C to 160 at 25 °C. The sorption of Pu to these materials appears to be stronger at 25 °C than that at 80 °C. Pu speciation may have affected this apparent sorption behavior. Pu oxidation state analysis using solvent extraction indicated that a much higher fraction of aqueous Pu(IV) existed in the intrinsic Pu colloid suspension at 25 °C than that at 80 °C (see section "K_d of Pu-clay and the thermodynamics" for more details), thus stronger sorption is expected from Pu(IV) species at 25 °C.

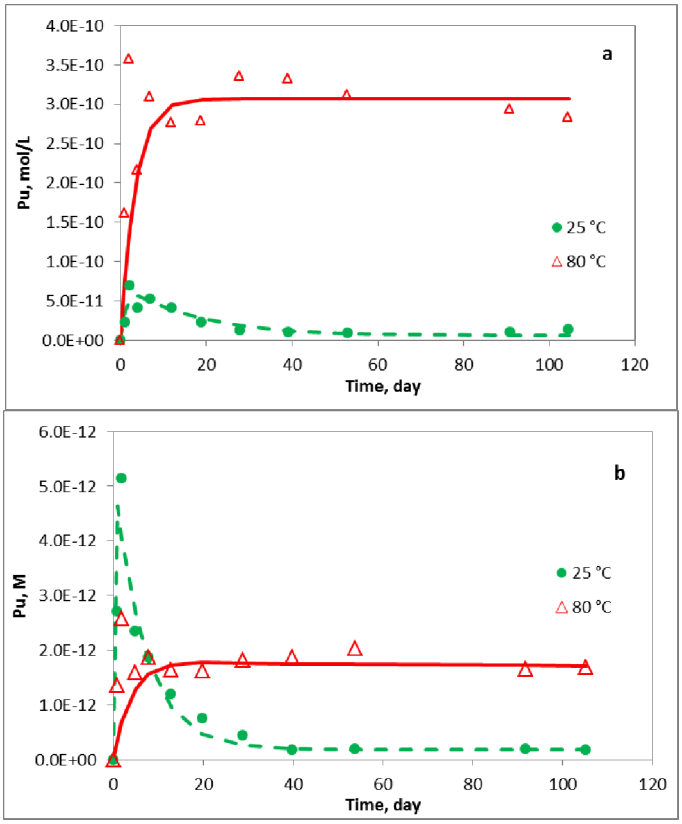

Fig. 6. Kinetics of Pu colloids and aqueous Pu^{4+} in the absence of montmorillonite at temperatures 25 and 80 °C. Solid circles (25°C) and open triangles (80 °C) are the experimental data points. Dash (25 °C) and solid lines (80 °C) are fitted curves using kinetics model psuedo1st order intermediate with equilibrium. 6a: Pu colloids-buffer systems, C^0= 9.13x10^{-10} mol/L; 6b: aqueous Pu(IV)-buffer systems, C^0=6.52x10-12 mol/L.

3.4 Temperature Effects

High temperature can enhance Pu(IV) hydrolysis as the process is endothermic(Altmaier et al., 2013; Cleveland, 1979). In addition, a significant increase in water ionization due to decreasing in pK_w (~ 12.50) at 80 °C also drives reaction towards Pu(IV) hydrolysis. As a result, the solubility of intrinsic Pu colloids under our experimental conditions decreased at higher temperature. A Pu(IV) solubility decrease in J-13 and UE-25p #1 groundwaters in the vicinity of Yucca Mountain, NV at elevated temperatures has also been reported despite possible existence of higher oxidation states of Pu(V, VI) and/or multi solid phases controlling Pu solubility(Efurd et al., 1998; Nitsche et al., 1993; Nitsche et al., 1994; Runde et al., 2002).

In general, the overall process of dissolution of a solid in an aqueous solution contains two essential steps: various chemical reactions occurring at the solid surface and the transport of dissolved species to and from the surface. The kinetics of the dissolution can be controlled by surface chemical reactions, transport of soluble species to and from the surface or a combination of both processes (Berner, 1981). The values of the dissolution activation energy (E_a) not only provide very important temperature dependence of the rate of dissolution, but also offer important clues to the dissolution mechanisms. According to Lasaga(Lasaga, 1998b), for mineral

dissolutions in water phase, typical values of E_a < 21 kJ mol^{-1} were for transport-controlled processes and E_a > 42 kJ mol^{-1} for the processes controlled by chemical reactions on solid surfaces. Intermediate values may be found for mixed-control (transport and surface) of the dissolution reaction (Hocsman et al., 2006). The relationship between a rate constant and the activation energy is described by Arrhenius equation:

$$k_1 = \boldsymbol{A_{diss}}\ exp(-\frac{E_a}{RT}) \qquad (12)$$

and E_a can be calculated using rate constants at two different temperatures:

$$\ln\left[\frac{k_1(T_2)}{k_1(T_1)}\right] = -\frac{E_a}{R}(\frac{1}{T_2} - \frac{1}{T_1}) \qquad (13)$$

where $\boldsymbol{A_{diss}}$ is the pre-exponential factor, which is a constant for a given reaction, $k_1(T_1)$ and, $k_1(T_2)$ are dissolution rate constant k_1 at absolute temperatures T_1 and T_2 in kelvin, respectively, E_a is the activation energy for the reaction, and R = 8.314 J mol^{-1} is the gas constant.
We used k_1 values obtained from low Pu colloids concentration experiments, in which the systems were far from solution equilibrium (exp. 1, 2, 5, 6), to calculate apparent E_a. The average of apparent activation energy (E_a) for PuO_2 colloids dissolution process was 28 kJ mol^{-1}. This intermediate value may indicate that the intrinsic Pu colloid dissolution process is controlled by a combination of both surface reaction and mass transport at the surface (Hocsman et al., 2006).

3.5 Temperature Dependence of Pu Sorption

The K_d values for Pu-montmorillonite can be calculated using the measured Pu activity on montmorillonite and in the supernatant. The resulting K_d values from the various experiments are plotted in Figure 7. Many factors including Pu speciation, oxidation state, and temperature can impact K_d values. Figure 7 indicates that at the same temperature, K_ds obtained from intrinsic Pu colloid experiments tend to have lower values than those obtained from aqueous Pu(IV) experiments. Furthermore, K_ds in intrinsic Pu colloids experiments increased over time to approach values from aqueous Pu(IV) experiments. This phenomenon can be explained by the change of Pu oxidation states during sorption processes. Pu(V) is the predominant species formed as a result of dissolution of intrinsic Pu colloids and this oxidation state exhibits a weaker sorption to clay relative to Pu(IV) (Altmaier et al., 2013; Begg et al., 2014; Neck et al., 2007a; Neck et al., 2007b). Over time, Pu(V) tends to reduce to Pu(IV) on the montmorillonite surface which leads to an increasing K_d over time (Begg et al., 2013b). Figure 7 also indicates that the K_d increases with temperature which implies that the sorption process is endothermic and that higher temperatures lead to greater Pu sorption to montmorillonite.

The van't Hoff equation as expressed in eq. 14 and Gibbs free energy as described in eq.15 can be used to calculate the changes in enthalpy (ΔH°, J mol^{-1}), entropy (ΔS°, J mol^{-1} K^{-1}) and Gibbs free energy (ΔG°, J mol^{-1}) of Pu-clay sorption at standard atmospheric pressure:

$$lnK_d = -\frac{\Delta H^\circ}{RT} + \frac{\Delta S^\circ}{R} \qquad (14)$$

$$\Delta G^\circ = \Delta H^\circ - T\Delta S^\circ \qquad (15)$$

where T is the absolute temperature in kelvin and R = 8.314 J mol^{-1} K^{-1} is the gas constant. The calculated thermodynamic parameters are summarized in Table 2. The positive value of ΔH° (38

kJ mol^{-1}) confirms endothermic nature of the Pu-clay sorption, and negative values of ΔG° indicate that the sorption reaction is spontaneous. A more negative value of ΔG° obtained from elevated temperature confirms that the Pu pseudo-colloids are more stable at higher temperature. However, as described in the following paragraph, the thermodynamic parameters derived from these experiment are only approximate since redox conditions, pH, and Pu oxidation states were not strictly controlled.

At the termination of the experiments, Pu oxidation state distribution in the supernatants of both intrinsic Pu colloids and Pu-clay pseudo colloids were analyzed using solvent extraction (Figure 8). We show that in the Pu-clay suspension, higher oxidation states PuO_2^+ and PuO_2^{2+} were the predominant species at 25 °C, while Pu^{4+} was more prevalent at 80 °C (Fig. 9a). This suggests that elevated temperatures led to more reducing solution conditions. This may, in part, explain the higher Pu K_ds at 80 °C. Although the Pu oxidation state distribution changed at different temperatures and colloidal solutions, and they made significant impact on the Pu sorption behavior, the processes controlling Pu speciation in solution or on mineral surface is not yet clear and requires further investigation.

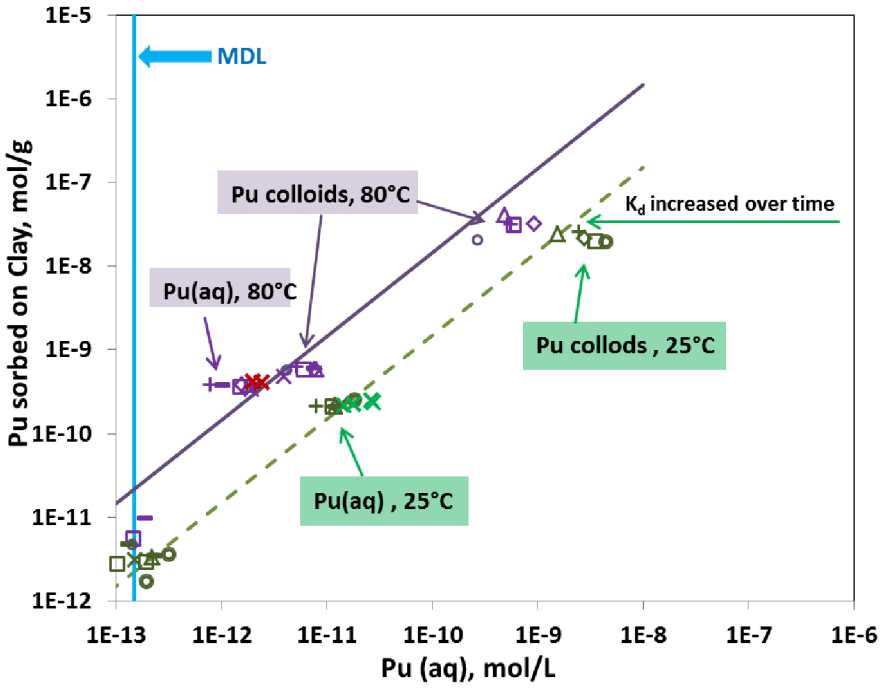

Figure 7. Pu sorption data from both colloidal and aqueous Pu(IV) experiments with montmorillonite at 25 and 80 °C. Dash (25 °C) and solid lines (80 °C) represent the average K_d values at each temperature.

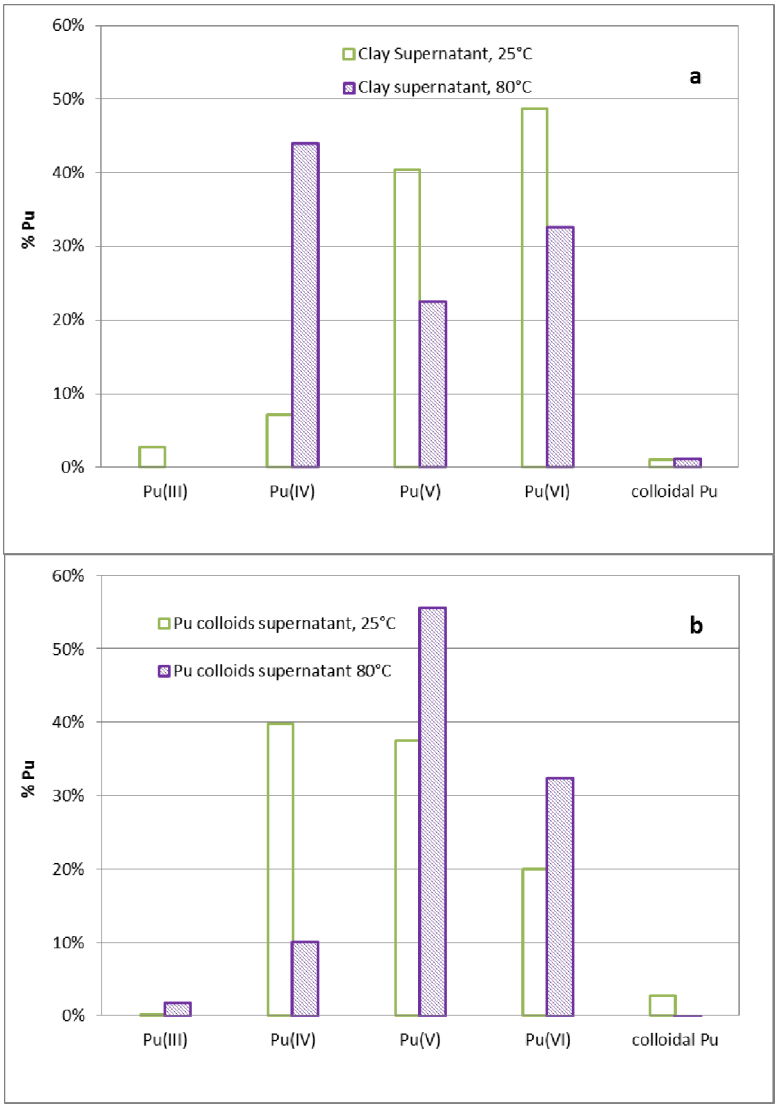

Figure 8. Pu oxidation states distributions at 25 °C(open bars) and 80 °C (filled bars). 9a. Clay supernatant outside of dialysis bag; 9b. Supernatant of Pu colloidal solution inside dialysis bag.

Table 2. Thermodynamic parameters for sorption of Pu onto montmorillonite at 25 and 80 °C.

Temperature	Average K_d (mL/g)	T (Kelvin)	ΔH°, kJ/mol	ΔS°, kJ/mol K	ΔG°, kJ/mol
25 °C	1.70E+04	298.15	38.0	0.21	-24.1
80 °C	1.85E+05	353.15	38.0	0.21	-35.6

4. Conclusions

A study of the dissolution of intrinsic Pu colloids in the presence of montmorillonite at different temperatures was successfully accomplished using a novel experimental setup containing a

dialysis device. This device enables us to separate two solid phases, but let them interact with each other via aqueous Pu ions. Kinetics of a series processes involved in intrinsic Pu colloid dissolution was modeled using 1st order reactions to compare the rate constant of different processes. We show that the kinetic constants for dissolution were one to two orders of magnitude lower than that of diffusion of aqueous Pu species in the system. Therefore the dissolution processes was the rate-limiting step. Although the presence of clay changes neither the colloids dissolution nor diffusion rates of Pu, it can stabilize dissolved Pu species and drive intrinsic Pu colloid dissolution and the formation of more stable Pu pseudo-colloids. Temperature enhances dissolution of intrinsic Pu colloids by overcoming a moderate activation energy (28 kJ mol^{-1}). Our thermodynamic study shows that the sorption of Pu on montmorillonite is endothermic as a positive change in enthalpy for the sorption has been obtained. The affinity of Pu for the clay increases with increasing of temperature resulting higher K_d at elevated temperature. The negative values of change of Gibbs free energy for Pu-clay sorption confirm that sorption of Pu onto clay occurs spontaneously and Pu pseudo-colloids are thermodynamically quite stable at both temperatures of 25 to 80 °C.

Although the fact that intrinsic Pu colloids tend to dissolve in the presence of montmorillonite may limit the migration of intrinsic Pu colloids, the subsequent formation of thermodynamically more stable Pu pseudo-colloids can play important role in Pu transport in the environment over significant temporal and spatial scales.

Part II: New Insights into Stability of Plutonium Intrinsic Colloids in the Presence of Clay at Elevated Temperatures II: Influence of Morphology on PuO_2 Reactivity

1. Introduction

PuO_2 dissolution is an important issue with respect to many fields including Pu transport behavior in the environment, storage and treatment of radioactive wastes from both laboratories and industries, and in reprocessing of spent nuclear fuels. From an environmental perspective, plutonium (Pu) is expected to be one of the dominant long-term dose contributors for high-level nuclear waste repositories because of its toxicity, long half-life (^{239}Pu half-life = 24.100 yrs.) and large inventory. In an effort to design a long-term barrier system for the safe disposal of nuclear waste, it is important to understand how Pu may migrate in the natural system once it breaches the waste package. Determining the fate and transport of Pu depends both on the initial chemical form at the source and the geochemistry and hydrology of the source location and along the down-gradient transport paths. Colloid-facilitated transport of low levels of Pu in both groundwater and surface water has been documented at several DOE sites (Dai et al., 2005; Kersting et al., 1999; Santschi et al., 2002a). Pu sorbed to iron oxide colloids has also been detected over 4 km from its original source in Mayak, Russia (Novikov et al., 2006). These field studies indicate that the Pu associated with mobile colloids has moved on the scale of kilometers, yet the mechanisms are not well understood. Without a conceptual understanding of the dominant processes and a quantitative understanding of the relevant reaction chemistry, current transport models cannot effectively predict Pu concentrations and transport rates in the field.

Pu can be associated with the colloidal fraction of groundwater in two different forms. Pu can migrate as either an intrinsic Pu colloids or sorb on to naturally occurring inorganic, organic or microbial species as pseudo-colloids. When concentrations of Pu exceed its solubility, Pu can hydrolyze to form intrinsic Pu colloids (Cleveland, 1979). In the case of Pu(IV), the solubility-limiting concentration may be as low as ~10^{-10} M under ambient conditions (Neck et al., 2007b). The transport of intrinsic Pu colloids will be controlled by their stability (both physical and chemical). In contrast, if concentrations of Pu ions are below their solubility, Pu ions can sorb on to naturally occurring colloidal forms including organic, inorganic, or microbial species resulting in the formation of Pu pseudo-colloids. The transport of Pu pseudo-colloids is determined by Pu sorption/desorption rates on the colloidal materials under given conditions. Efforts to model the transport of Pu from a near-field to a far-field environment are currently limited due to the lack of understanding of how intrinsic Pu colloids will persist along a changing geochemical flow path away from a high-level nuclear waste repository where intrinsic Pu colloids are most likely to form (Kersting, 2013).

In addition to a broad range of geochemical processes and conditions (e.g. temperature, Eh / pH, isotopic composition) that can affect the overall stability of intrinsic Pu colloids once they are formed, the initial formation conditions also play a critical role in their long-term stability. The morphology of a solid phase including crystal structure, the crystallite size and aggregation is among the important factors that greatly influences the reactivity of the solid. Previous investigations on intrinsic Pu colloids showed that the ultimate morphology is strongly dependent on the conditions of formation and age of solution (Walther and Denecke, 2013). In particularly, the degree of crystallinity, which can be affected by aging, temperature and original formation conditions, will affect the stability of intrinsic Pu colloids (Farr et al., 2004; Haire et al., 1971;

Rai and Ryan, 1982; Runde et al., 2002). Published thermodynamic data for Pu(IV) oxide and hydroxide show a range of $pK_{s,0}$ for PuO_2(hyd) and PuO_2(cr) from 50.2 to 58.8 and 60.2 to 64.0, respectively (Lemire, 2001). These data illustrate how crystallinity can have a significant impact on the solubility and stability of PuO_2.

In the current study, we performed long-term dissolution experiments of three different forms of intrinsic Pu colloids in the presence of montmorillonite at two different temperatures. All three intrinsic Pu colloids used were formed under elevated temperature conditions. The results are compared to experiments performed with hydrous Pu dioxide prepared in a weak alkaline solution at room temperature and reported in Part I of this report. Scanning electron microscopy (SEM) and transmission electron microscopy (TEM) were used to characterize the morphology of intrinsic Pu colloids including crystal structure, orientations of single crystallites within PuO_2 aggregates and particle sizes. The combination dissolution experiments and morphology characterization of intrinsic Pu colloids was used to identify the impact of PuO_2 formation conditions, morphological characteristics, and crystallinity on the stability of PuO_2 solid phases.

2. Material and Methods

All reagents were of analytical grade or better and used as received. De-ionized water from a Barnstead Milli‑Q Water (MQW) purification system (resistivity: 18.2 megaohm-cm) was used for all procedures and solution preparation.

2.1 Calcination of High-Fired ^{239}Pu Oxides

Reactor fuel grade Pu oxide was used to make the high-fired Pu oxides. The Pu isotopic ratios in mass percentage for ^{238}Pu, ^{239}Pu, ^{240}Pu, ^{241}Pu and ^{242}Pu were 0.046%, 88.0%, 11.6%, 0.25% and 0.065%, respectively. The starting material was dissolved in concentrated nitric acid containing a small admixture of HF. After filtering, Pu was converted to the +3 oxidation state using hydroxylamine (NH_2OH) in dilute nitric acid. Pu(III) was then precipitated by the addition of oxalic acid to form Pu(III) oxalate. The precipitate was allowed to settle for 30-60 minutes, filtered, washed with DI water, alcohol, and then dried under vacuum at room temperature. The dried Pu(III) oxalate was then calcined at temperatures of either 300°C (high-fired PuO_2 #1) or 800°C (high-fired PuO_2 #2) to convert Pu(III) oxalate to PuO_2. To prepare samples for our dissolution experiments, the Pu dioxide powders were suspended in Milli-Q water, allowed to settle for 10 minutes. The supernatant, including PuO_2 fines, was discarded. This Milli-Q water rinse was repeated three times. The Pu concentration of the two high-fired Pu dioxide suspensions was determined by ^{241}Pu using beta liquid scintillation counting (LSC). For logistical and safety reasons, the two high-fired Pu dioxides prepared in this manner were not colloidal sized. Grinding these samples to produce colloid-sized particles was not practical due to sample dispersal safety concerns. However, in this report, we refer to these samples as intrinsic Pu colloids.

2.2 Peptization of PuO_2 Colloidal Sols

A ^{242}Pu stock solution consisting of alpha emitters ^{238}Pu, ^{239}Pu, ^{240}Pu, and ^{242}Pu with activity percentages of 15.8%, 0.062%, 5.0%, and 79.1%, respectively, was purified using an AG1x8 100-200 mesh anion exchange resin column. The intrinsic Pu colloids were prepared by heating 1.6×10^{-3} M Pu(IV, aq) in 0.1 M HNO_3 solution on a hotplate at 60-80 °C for 30 min. The dark brown Pu(IV) solution turned to a green color immediately upon heating. The formation of

intrinsic Pu colloids was confirmed by UV/VIS. The fraction of soluble Pu in the intrinsic Pu colloid solution was determined to be < 0.2% using a 3kDa NMWL (Nominal Molecular Weight Limit) ultra-centrifugal filter. After aging for two years, a dilution of the intrinsic Pu colloids (Pu concentration of 3×10^{-5} M) was made in pH 8 buffer solution (5 mM NaCl/0.7 mM $NaHCO_3$) and used in our experiments.

2.3 Precipitation of Intrinsic Pu Colloids in an Alkaline Solution

A relatively pure alpha-emitting ^{238}Pu stock solution was used in low- and intermediate-Pu-concentration experiments. The isotopic ratios in mass percentage for ^{238}Pu, ^{239}Pu, ^{240}Pu, and ^{241}Pu were 76.83%, 21.03%, 2.01%, and 0.142%, respectively. The major isotope contributing to alpha activity in this stock was ^{238}Pu (~99.9% by activity). Pu stock solution was purified using AG®1-×8 100-200 mesh anion exchange resin from Bio-Rad Laboratories, and filtered through an Amicon Ultra 0.5 mL centrifugal filter with membrane MWCO of 3 kDa from EMD Millipore. The intrinsic Pu colloids were prepared by neutralizing Pu(IV) stocks using NaOH solution and adjusting solution pH to pH 9−10. After aging for more than a week, the intrinsic Pu colloids were centrifuged at an RCF of 9168 × g for 1 hr, and the supernatant was removed. The intrinsic Pu colloid particle size cut-off based on centrifugation was 14 nm. The intrinsic Pu colloids were re-suspended in Milli-Q water. The intrinsic Pu colloid starting solutions were prepared by adding a spike of intrinsic Pu colloids into the pH 8 buffer solution without further pH adjustment. Pu concentrations in samples were analyzed by a PerkinElmer Tri-Carb 2900TR Liquid Scintillation Analyzer. The concentration of soluble Pu in the intrinsic Pu colloid starting solutions, measured in 3kDa NMWL filtrate were 1~3% of the total concentrations.

2.4 Preparation of Montmorillonite

SWy-1 Montmorillonite from the Clay Minerals Society was used in our experiments. Detailed summary on the preparation of the homo-ionic Na-montmorillonite can be found in (Begg et al., 2013b), and then the prepared clay minerals were suspended in Milli-Q water and centrifuged to obtain the fraction of particle sizes from 50 nm to 2 microns (see detailed description in Part I of this report).

2.5 Determinations of Pu Concentrations

Two different Pu sources (^{242}Pu and reactor fuel grade ^{239}Pu) were used in this study. For the intrinsic Pu colloids made from ^{242}Pu stock solution, alpha liquid scintillation counting (LSC) was used to determine Pu concentrations. The reactor fuel grade Pu dioxide contained ^{241}Am, the daughter of ^{241}Pu, as a predominant alpha emitter, which contributed > 90% of the total alpha activity in the samples. It was not possible to use alpha LSC to quantify Pu concentrations in our dissolution experiments. Therefore, beta LSC was used to measure activity of ^{241}Pu in samples, and Pu isotopic ratios were used to determine the total Pu concentrations in the samples. For beta LSC quantification, a ^{241}Pu quenching curve was generated from a NIST traceable standard and used to determine the LSC counting efficiency for each sample.

2.6 Dialysis Experiments

In the context of this report, we have chosen to refer to all solid phase plutonium oxides used in these experiments as intrinsic Pu colloids. As will be shown in the SEM images, some forms of plutonium oxides were not colloidal sized. In some cases, plutonium oxide aggregates were not colloidal-sized but the individual crystallites that formed the aggregates were colloidal-sized. Detailed morphological characterization of the various samples are provided in the following sections. However, in the discussion, we broadly define all plutonium oxides used in these experiments as intrinsic Pu colloids.

A total of 7 dialysis experiments were performed to investigate the stability of intrinsic Pu colloids in the presence of montmorillonite and compared to the results from previous experiments (see part I of the report). Experiments were performed at 25 °C (4 experiments) and 80 °C (3 experiments) to evaluate the effect of temperature on colloid stability of these intrinsic Pu colloids. The experimental conditions and parameters are listed in Table 1. All batch experiments were conducted in 450-mL Teflon jars with air-tight closures. A sealed dialysis bag containing 15 mL of an intrinsic Pu colloid suspension was placed in the 250 mL of pH 8 montmorillonite suspension with a solid to liquid ratio of 1g : 1L. The 450-mL Teflon jars were submerged in 1-L Teflon containers filled with Milli-Q water to minimize evaporative losses and provide secondary containment to the radioactive samples. Over the course of the experiment, the 25°C samples were placed on a top-loading orbital shaker, and the 80 °C samples were submerged in a heated water bath (Innova 3100) and shaken at an orbital speed of 100 rpm. Pu concentrations in the clay suspension outside of dialysis bag were monitored as functions of time over a six-month or longer period. At each sampling interval, aliquots of the montmorillonite suspension were collected and analyzed for total Pu. At the termination of the experiments, total Pu concentrations in the clay suspensions were measured. The pH of the clay suspension was monitored and maintained at pH 8 ± 0.5 at all times.

Table 1. Conditions of intrinsic Pu colloid stability experiments at 25 and 80 °C.

Expt	Expt. Temp.	Pu oxides used	PuO_2 formed temperature	Initial Pu conc. inside dialysis bag	Pu upper limit in clay susp.	Montmorillonite suspension	MWCO
	°C		°C	mol L^{-1}	mol L^{-1}	g L^{-1}	kDa
1	25	high-fired PuO_2 -1	calcined at 300	3.6×10^{-6}	2.7×10^{-7}	1	1000
2	25	high-fired PuO_2 -1	calcined at 300	2.2×10^{-7}	2×10^{-8}	1	500 -1000
3	25	high-fired PuO_2 -2	calcined at 800	1.1×10^{-6}	6×10^{-8}	1	1000
4	25	peptized PuO_2 -3	peptized in dilute acid at 70	3.9×10^{-5}	3.6×10^{-6}	1	500 -1000
5	80	high-fired PuO2 -1	calcined at 300	4.9×10^{-8}	2.8×10^{-9}	1	1000
6	80	high-fired PuO2 -2	calcined at 800	3.9×10^{-6}	2.2×10^{-7}	1	1000
7	80	peptized PuO_2 -3	peptized in dilute acid at 70	1.4×10^{-6}	8×10^{-8}	1	1000

2.7 Instrumentation

Intrinsic Pu colloids and high-fired Pu oxides were characterized using scanning electron microscopy (SEM) and transmission electron microscopy (TEM) for their morphology, crystal structure and chemical composition. SEM analysis was performed using a JEOL 7401-F field emission scanning electron microscope equipped with an Everhart-Thornley secondary-electron detector and a solid state backscattered electron detector for imaging. The SEM is also equipped with an Oxford X-Max (80 mm2) silicon drift detector and Oxford Aztec software to perform X-ray energy dispersive spectroscopy (EDS) measurements of chemical elements. TEM was performed using a Philips CM300-FEG transmission electron microscope with a field emission electron gun operating at 300 kV. The CM300-FEG microscope is equipped with an Oxford X-

ray detector for EDS measurements. Solution UV/Vis spectra were taken from Cary 500 Scan UV-Vis-NIR spectrophotometer. Liquid scintillation counting was performed on a PerkinElmer Tri-Carb 2900TR liquid scintillation analyzer.

3. Results and Discussion

3.1 Characterization

SEM and TEM images of three different types of intrinsic Pu colloids prior to dissolution experiments were obtained to compare their morphologies and particle sizes. Figure 1a and 1c show general morphology of the intrinsic Pu colloid samples in low magnified SEM images. An average particle size of 4 µm was observed by SEM for the two high-fired samples. However, high-fired PuO_2 -1 contained a significant number of smaller particles that were submicron in sizes. It is observed that the variation of particle sizes was closely related to calcination temperatures (fig. 1b and d). PuO_2 formed by calcination at lower temperature showed significant spreading of particle size distribution. However, the mass distributions of the PuO_2 as function of particles sizes were not very sensitive to the calcination temperatures (Machuron-Mandard and Madic, 1996). Our observations are consistent with the findings reported by Machuron-Mandard and Madic. Both samples contain highly porous and layered square platelets. The higher magnified SEM images (fig. 1b and 1d) show that these square platelets are polycrystalline in nature and consist of individual crystallites with size distribution range from a few nanometers to >300 nm. Sample PuO_2-1 calcined at 300 °C shows a wide spreading grain size distribution (fig. 1b) ranging from a 4 to > 300 nm. The average particles size was estimated to be 5 nm for high-fired PuO_2-1 due to predominance of particle sizes <10 nm. This estimation was based on size measurements for particles of >10 nm and area measurements for particles of <10 nm from SEM images. On the other hand, high-fired PuO_2-2 calcined at 800 °C exhibits a much more uniform size distribution with majority of the crystallite sizes within a narrow range of 20-50 nm. The average particle size for high-fired PuO_2-2 was measured to be 31 nm by SEM image analysis. Our TEM observations (not shown here) also confirmed this result.

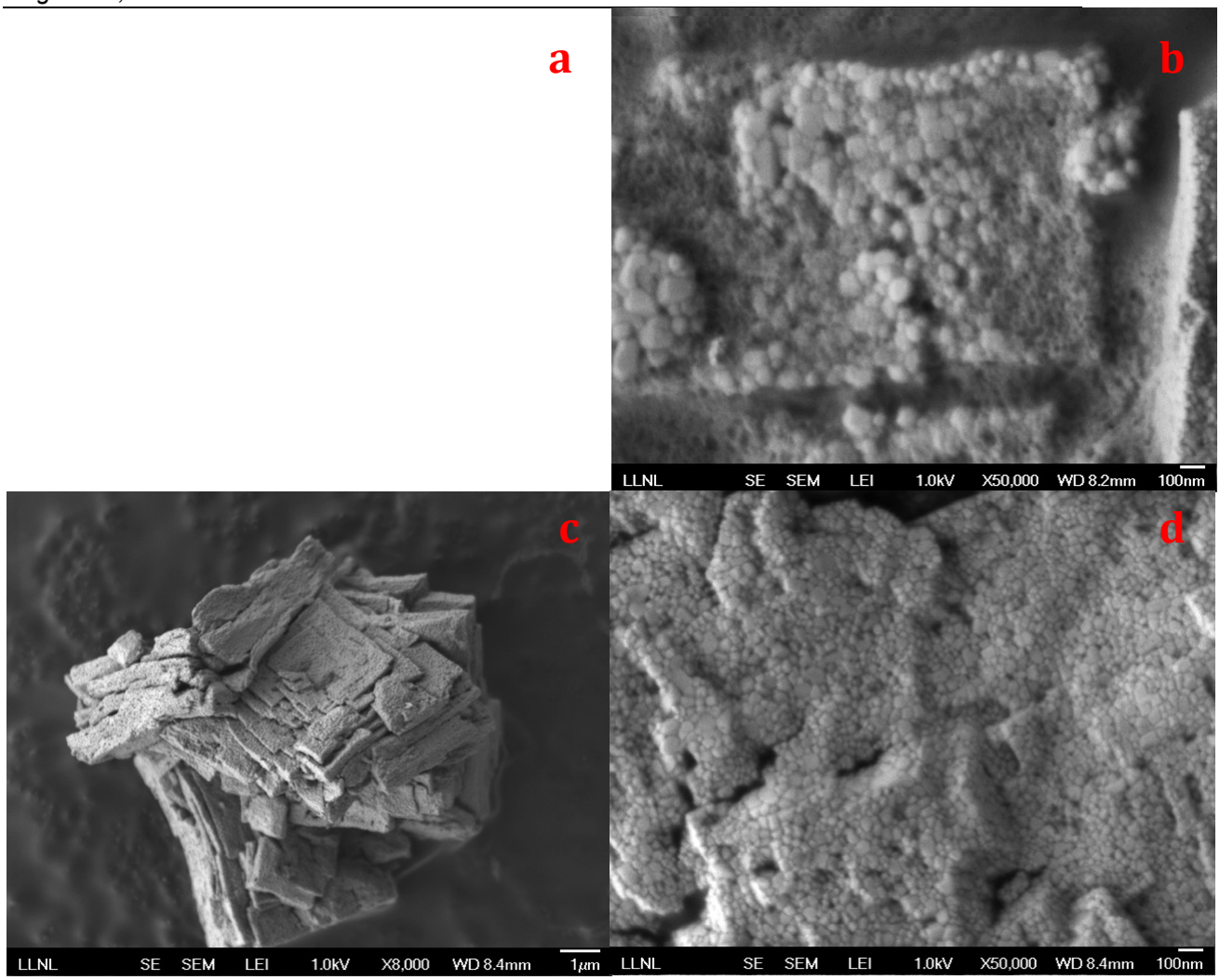

Figure 1. Secondary electron SEM observations of high-fired PuO_2 particles. 1a. PuO_2 calcined at 300 °C forming layered porous square platelets with uneven grain size distribution. 1b. High magnification image of PuO_2 calcined at 300 °C showing wide range of grain size distribution from few nanometers to > 100 nm. 1c PuO_2 calcined at 800 °C forming layered porous square platelets with relative even grain size distribution. 1d High magnification image of PuO_2 calcined at 800 °C showing majority of grain sizes distribute between 20-50 nm.

Figure 2 shows transmission electron microscopy (TEM) observations of intrinsic Pu colloids prepared by either peptization of Pu hydroxide colloidal sol in 0.1 M HNO_3 solution or precipitation from weak alkaline solution of pH 9~10. The intrinsic Pu colloids peptized in dilute nitric acid solution are well defined spherical aggregates of PuO_2 single crystallites. The measured average size of the aggregates was 31 nm, while the measured average size of individual PuO_2 crystallites in each aggregate was 2.5 nm. The electron diffraction spectrum (EDS) of peptized intrinsic Pu colloids matched typical PuO_2 FCC crystal structure. Although the individual crystallites form rough outer surface of the aggregates, HRTEM image of one aggregate (Fig. 2b) reveals that individual crystallites fuse together and exhibit a preferential crystal structure orientation. This is the first time that we report the image of this quasi-single-crystal structure in intrinsic Pu colloids. This unique character may cause peptized PuO_2 aggregates to share some features of larger single crystals. On the other hand, intrinsic Pu colloids

precipitated from alkaline solution flocculated in solution formed aggregates with poorly defined shapes (see Fig. 2c). These aggregates also consist of individual PuO_2 crystallites of sizes 2.5-4.5 nm (see Fig. 2d), however, the individual crystallites didn't show any preferred crystal structure alignment within the aggregates. Instead, they exhibit completely random orientations (Fig. 2d). Neither the freshly prepared nor the aged intrinsic Pu colloids prepared in a alkaline solution (up to 1 year) showed any change in their crystallite orientations. The various intrinsic Pu colloids used in these experiments have different particle sizes and ultimately different surface areas. Due to the health and safety concerns inherent in working with potentially dispersible Pu powders, the high-fired Pu oxides could not be ground to finer sizes. The surface area of these Pu oxides/colloids was estimated based on the sizes of crystallites as well as the sizes of the aggregates and the data are tabulated in Table 2. It is noticeable that specific crystallite surface area of samples PuO_2-1, PuO_2-3 and PuO_2-4 were similar within a range of 104 to 227 $m^2\ g^{-1}$and the ones for PuO_2-2 was one order of magnitude smaller. On the other hand, samples PuO_2-1 and 2 have same specific particle surface area of ~0.1 m^2/g^{-1}, while samples PuO_2-3 and 4 have similar specific particle surface area around ~20 $m^2\ g^{-1}$. Due to limited quantities of the materials, BET measurements were not performed for these tested samples. However, PuO_2 surface areas have been measured previously and the measured values are in the range of 1.2 to 12.3 $m^2\ g^{-1}$ (Machuron-Mandard and Madic, 1996) at calcination temperatures from 1050 to 450 °C, and 5 to 41 $m^2\ g^{-1}$ for PuO_2 treated at 1750 °C (Mewhinney et al., 1987), respectively. These measured specific areas are equivalent to particle size ranges of 43 ~ 430 and 13 ~ 100 nm, respectively, which more or less reflect the sizes of Pu oxides aggregates used in our study.

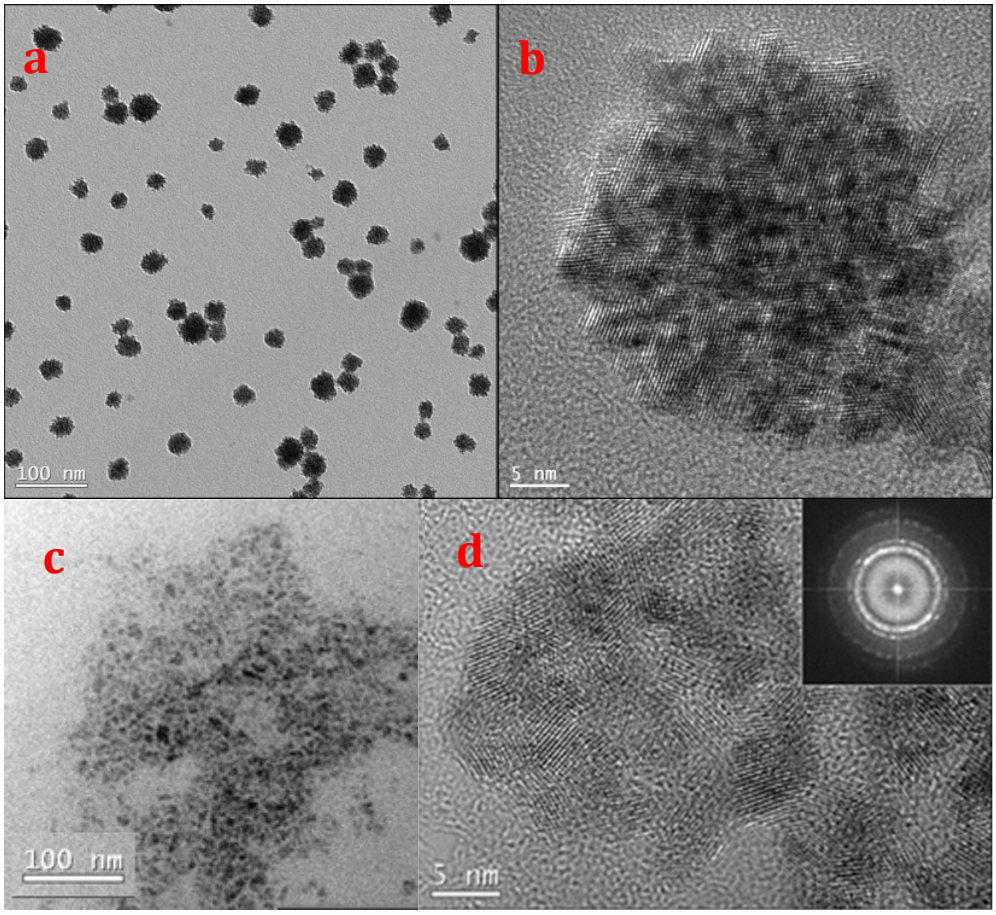

Figure 2. Bright-field TEM images of Pu-colloids. a. Dispersed spherical PuO_2 clusters formed by peptization in dilute nitric acid solution. b. HRTEM images of one peptized PuO_2 polycrystalline cluster with 2-3 nm sized individual crystallites. These individual crystallites exhibit a preferential crystal structure orientation. c. Flocculated PuO_2 with irregular shape formed by precipitation of Pu(IV) in weak alkaline solution.d. HRTEM images of one precipitated PuO_2 particle showing polycrystalline structure with 2-5 nm individual crystallites. Individual crystallites exhibit random crystal structure orientation. The inset electron diffraction pattern shows FCC crystal structure of PuO_2.

Table 2. Particle sizes and surface area of intrinsic Pu colloids and montmorillonite used in this study.

Intrinsic Pu colloid/clay	Density	Crystallite			Aggregate		
		Avg Diameter	Diameter Range	Surface Area	Avg Diameter	Diameter Range	Surface Area
	g/cm^3	nm	nm	m^2/g	nm	nm	m^2/g
High-fired PuO_2 #1 (PuO_2-1)	11.5	5	3-335	104	4000	0.1-10	0.13
High-fired PuO_2 #2 (PuO_2-2)	11.5	31	10-105	17	4000	2-10	0.13
Peptized $^{242}PuO_2$ (PuO_2-3)	11.5	2.3	2-3.1	227	31	16-50	17
Precipitated $^{238}PuO_2$ (PuO_2-4)	11.5	3.5	2.5-4.5	149	30	10-50	17
Montmorillonite[a]	2.83	71		30	300	50-2000	7

a. N_2(g)-BET measurement was 31.45 ± 0.17 m2/g

3.2 Dissolution of Intrinsic Pu Colloids

The kinetics studies of intrinsic Pu colloids precipitated from weak alkaline solution (both freshly prepared and aged up to 1 year) was studied in the presence of montmorillonite at 25 and 80 °C previously (Part I of this report: kinetics studies). Colloid stability at three different intrinsic Pu colloid concentrations (10^{-11}, 10^{-9} and 10^{-7} M) was examined. These intrinsic ^{238}Pu colloids were aged for 1 month to >1 year prior to use in the stability experiments. However, no difference in behavior was observed between the fresh and aged samples. The dissolution rate constants obtained from those experiments were ranged from 6×10^{-7} to 1×10^{-5} and 4×10^{-7} to 7×10^{-7} mol m^{-2} day^{-1} at 25 and 80 °C, respectively. We have found that the apparent dissolution rates in our experiments were a function of the formation conditions of the intrinsic Pu colloid, intrinsic Pu colloid surface area and colloids concentration, and solution temperature. Although 7 experiments using calcined PuO_2 and peptized Pu hydroxide colloids were performed in over prolonged periods from 6 month to 8 months (see Table 1), only two experiments (exp. 4 and 6) showed signs of intrinsic Pu colloid dissolution. Figure 3 plots the Pu concentration in the clay suspension as function of time for these two experiments. In contrast to our previous intrinsic Pu colloid dissolution (Pu hydroxides precipitated in alkaline solution) in which nearly complete dissolution was achieved in three months, Pu concentrations in these experiments were detectable in clay suspensions only after ~100 days, implying very slow dissolution kinetics. A first order reaction model was applied to the data obtained from exp. 4 and 6, and could only qualitatively fit the dissolution curves (see Figure 4), especially for exp. 6. The rate constants obtained from curve fitting were 1.6×10^{-7} and 1.7×10^{-8} mol m^{-2} day^{-1} for samples PuO_2-3 at 25 °C (exp. 4) and PuO_2-2 at 80 °C (exp. 6), respectively. These values were 1 to 2 orders of magnitude lower than those obtained from experiments using sample PuO_2-4 (precipitated PuO_2 in alkaline solution). Given that the specific crystallite surface area of PuO_2-3 is even slightly higher than that of PuO_2-4, and both samples had very similar specific particle area, the observed difference in dissolution rate was more likely due to the difference in their morphologies, especially the degree of crystallinity. The higher the degree of crystallinity, the more stable the intrinsic Pu colloids, and thus, lower dissolution rate was observed. Sample PuO_2-2 appeared to dissolve at 80 °C, although it had highest degree of crystallinity with smallest specific crystallite surface areas. Again the observed dissolution could not be explained by its surface area. Without additional experimental information and further investigations, we are unable to give a satisfactory explanation for this result.

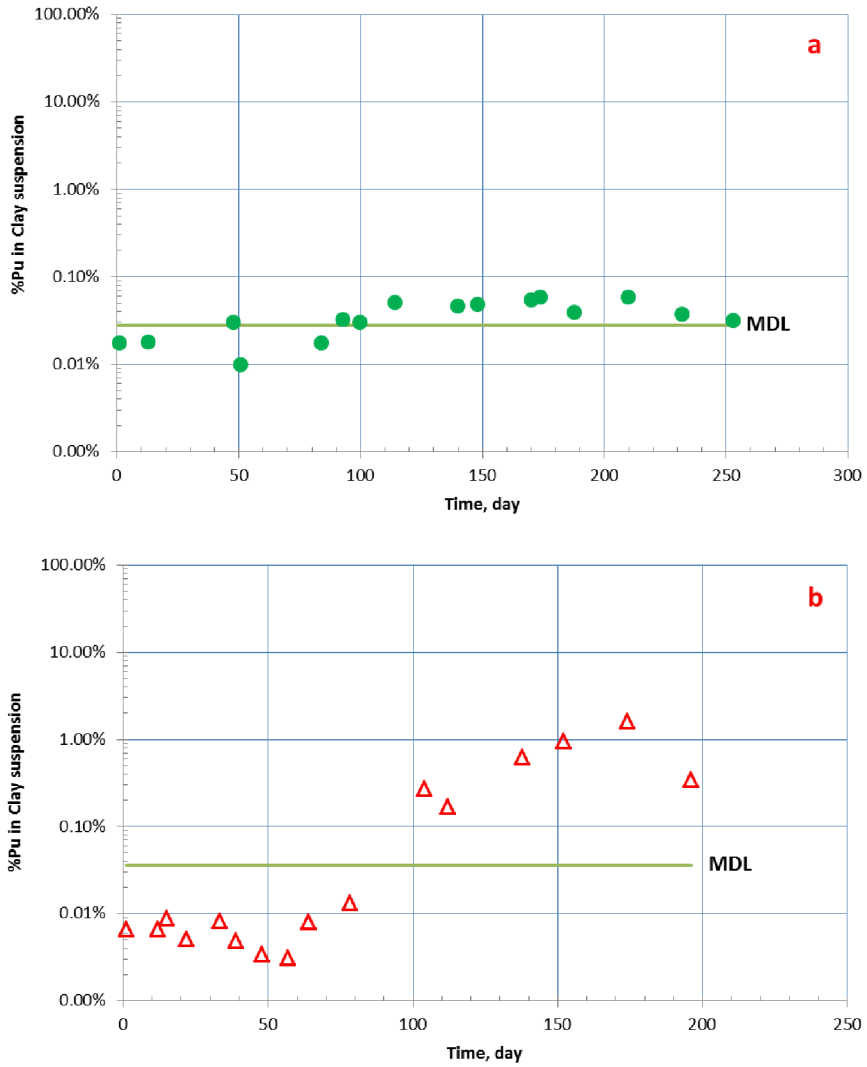

Figure 3. Dissolution kinetics of intrinsic Pu colloids. Solid circles and open triangles are experimental data at 25 and 80 °C, respectively. Solid lines are the method detection limits (MDL). a. Dissolution of peptized $^{242}PuO_2$ at 25 °C. b. Dissolution of calcined $^{239}PuO_2$ at 80 °C.

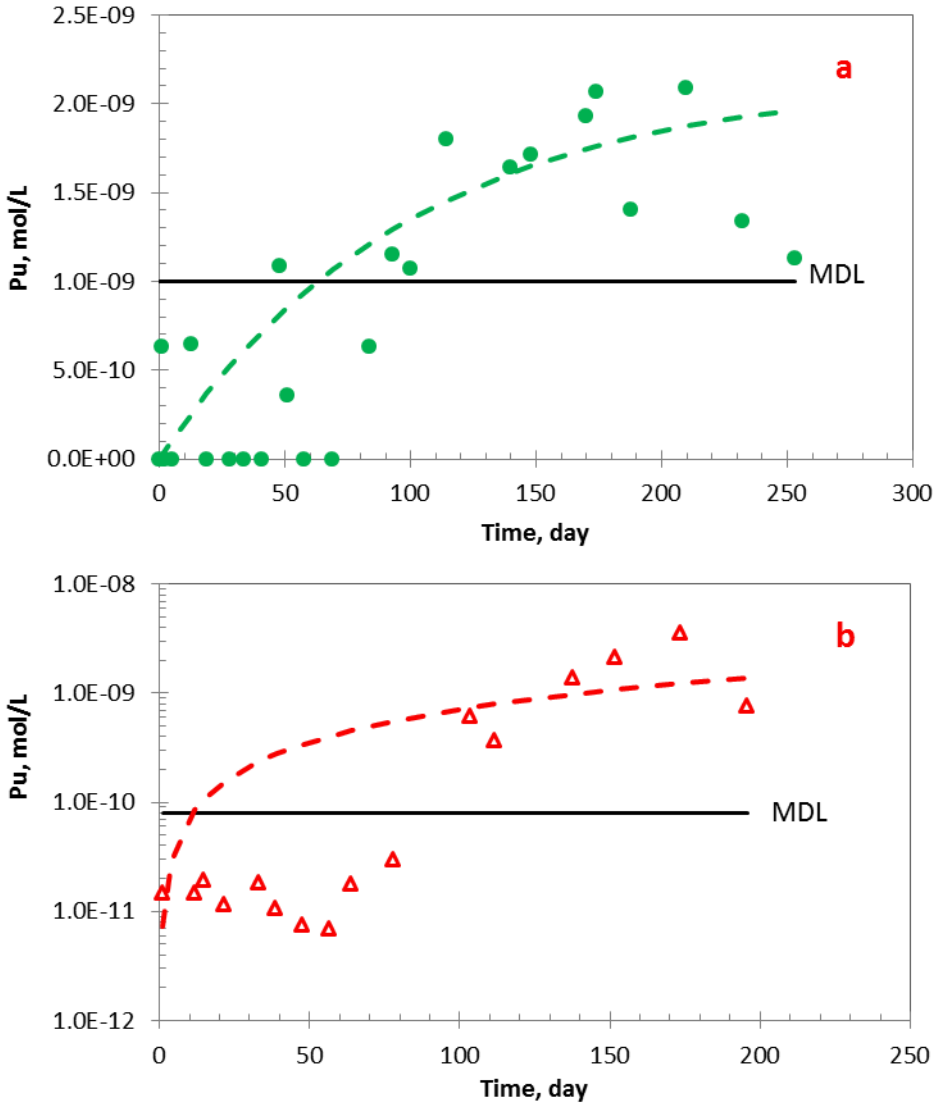

Figure 4. Dissolution kinetics were modeled using a first order reaction model. Solid circles and open triangles are experimental data at 25 and 80 °C, respectively. Solid lines are the method detection limits (MDL), and dashed lines are model fitting curves. a. Dissolution of peptized $^{242}PuO_2$ at 25 °C. The obtained dissolution rate constant was 1.6×10^{-7} mol/m^2/day. b. Dissolution of calcined $^{239}PuO_2$ -2 at 80 °C. The obtained dissolution rate constant was 1.7×10^{-8} mol/m^2/day.

Conservative predictions of Pu concentrations in the clay suspension were calculated using the dissolution rate constants obtained from sample PuO_2-4 and the estimated crystallite surface areas of each of the intrinsic Pu colloids tested. The resulting Pu dissolution rates were compared to experimental results. These results are summarized in Table 3. For all cases, the predicted Pu concentrations are higher than either measured Pu concentrations in clay suspensionor MDLs for the individual experiments. Moreover, the TEM observations (not shown here) fromsample

PuO_2-3 at the end of the dissolution 25 and 80 °C experiments did not show any significant signs of dissolution. All these results confirm that the dissolution rates of samples PuO_2-1 to 3 were much slower than that of PuO_2-4. Aside from crystallinity considerations, radiation effects from ^{238}Pu have also been reported to damage the crystallinity of ^{238}Pu oxides which led to an increased solubility of $^{238}PuO_2$ (Park et al., 1973). The combined amorphous nature of the intrinsic Pu colloids and the high ^{238}Pu activity leads to the highest dissolution rates in sample PuO_2-4. However, further experiments of the radiation effects are needed to quantitatively compare Pu oxides dissolution behavior and processes.

Table 3. Summary of dissolution experiment results, MDL and Pu conc. at the termination of experiments

Expt	Expt Temp.	PuO_2 used	Crystallite diameter	Calculated surface area	Pu upper limit in clay suspension	Apparent min k_s from previous expt	Expt duration	MDL	Measured final Pu conc.	Predicted Pu conc.
	°C		nm	$m^2\ mol^{-1}$	$mol\ L^{-1}$	$mol\ m^{-2}\ day^{-1}$	day	$mol\ L^{-1}$	$mol\ L^{-1}$	$mol\ L^{-1}$
1	25	PuO_2-1	5	2.8×10^{4}	2.7×10^{-7}	6.2×10^{-7}	196	6×10^{-11}	1.5×10^{-8} [a]	2×10^{-8}
2	25	PuO_2-1	5	2.8×10^{4}	2×10^{-8}	6.2×10^{-7}	252	6×10^{-11}	< MDL	2×10^{-9}
3	25	PuO_2-2	31	4.6×10^{3}	6×10^{-8}	6.2×10^{-7}	196	6×10^{-11}	1.5×10^{-9} [b]	3×10^{-9}
4	25	PuO_2-3	2.3	6.2×10^{4}	3.6×10^{-6}	6.2×10^{-7}	253	3×10^{-10}	2.5×10^{-9} [c]	4×10^{-7}
5	80	PuO_2-1	5	2.8×10^{4}	2.8×10^{-9}	3.7×10^{-6}	191	6×10^{-11}	< MDL	4×10^{-10}
6	80	PuO_2-2	31	4.6×10^{3}	2.2×10^{-7}	3.7×10^{-6}	196	6×10^{-11}	4.5×10^{-9} [c]	3×10^{-8}
7	80	PuO_2-3	2.3	6.2×10^{4}	8×10^{-8}	3.7×10^{-6}	182	3×10^{-10}	< MDL	1×10^{-8}

a. Pu concentration was not detected for 140 days, and then it jumped to this value on 150 days and stayed on it to the termination of the experiment. It is concluded that the detected Pu was due to the decay of the integrity of dialysis membrane after a long-lasting experiment.

b. Pu concentration was not detected for 170 days, and then it jumped to this value on last sampling day. It is concluded that the detected Pu was due to the decay of integrity of the dialysis membrane after a long-lasting experiment.

c. Dissolution of PuO_2 may have been observed in these experiments.

3.3 Temperature Effects on PuO_2 Morphology and Reactivity

Intrinsic Pu colloids were retrieved from inside dialysis bags after the dissolution experiments (exp. 4 and 7) for TEM imaging (Fig. 5). The HRTEM images of the samples revealed that the aggregates tend to fuse at their edges with a preferential alignment in the 25 °C experiment (Fig. 5a). The signs of particle fusion were not as developed at 80 °C (Fig. 5b). These observations indicate that PuO_2 aggregates exhibit stronger relationship with each other at 25 °C than that at 80 °C. It suggests that intrinsic Pu colloids are more reactive at 25 °C. These observations may explain why we observed some intrinsic Pu colloids dissolution at 25 °C, but not at 80 °C for sample PuO_2-3.

In the current study, we show that intrinsic Pu colloids formed at elevated temperatures resulted in greater crystallinity and larger single crystals (PuO_2-1 and PuO_2-2 in Fig. 1). In the liquid phase, temperature effects led to intrinsic Pu colloids forming well defined aggregate shapes and the incipient alignment of the crystallites within the aggregates (PuO_2-3 compared to PuO_2-4 in Fig. 2). These features likely reduced the surface energy and surface reactivity of the intrinsic Pu colloids. Thermal treatments have been shown to be one of the very important factors influencing PuO_2 surface chemistry including its reactivity and heterogeneous dissolution kinetics (Farr et al., 2004). Increasing temperatures can effectively decrease Pu oxides solubility in groundwaters (Nitsche et al., 1993; Runde et al., 2002). The temperature effect on intrinsic Pu colloids was attributed to the increased crystallinity of the solubility controlling solids (Runde et al., 2002) and crystal growth (Machuron-Mandard and Madic, 1996) during formation of PuO_2. It is apparent

from our experiments that intrinsic Pu colloids formed at elevated temperatures are more stable and less reactive than those formed at room temperature. The various formation temperatures influence morphological features including crystallinity, crystal growth, aggregation and particle shapes and sizes. These morphological difference will have a substantial effect of the stability and dissolution rates of intrinsic Pu colloids.

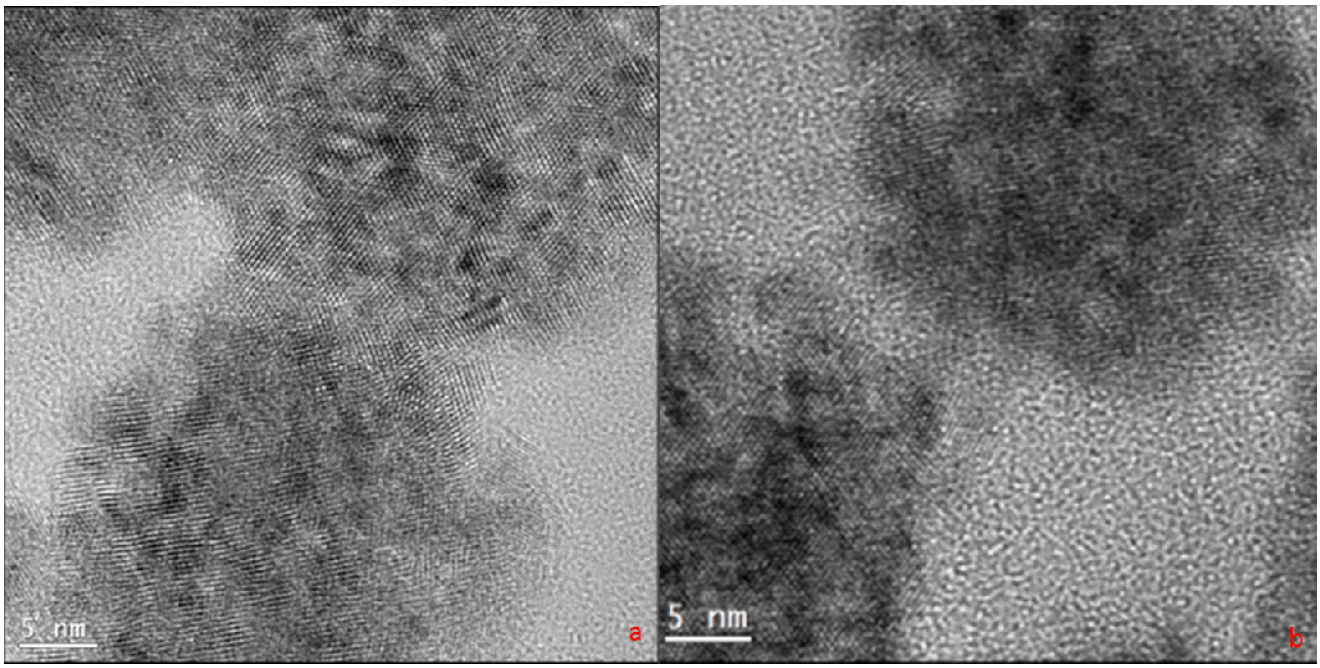

Figure 5. HRTEM images of sample PuO_2-3 from inside dialysis bag after dissolution experiments. a: Sample from experiment at 25 °C. The aggregates tend to fuse at their edges with preferential alignment. b: Sample from experiment at 80 °C. The aggregates show minimum fusion at their edges.

4 Conclusions

We have examined the reactivity of three different types of intrinsic Pu colloids in the presence of montmorillonite at 25 and 80°C under atmospheric conditions. Scanning electron microscopy (SEM) and transmission electron microscopy (TEM) have been used to characterize their morphology. Pu oxides calcined at 300 and 800 °C and intrinsic Pu colloids produced from acidic solution are quite stable under our experimental conditions. Only two out of seven experiments showed signs of intrinsic Pu colloid dissolution after 100 days. Predicted Pu concentrations calculated using dissolution rate constants obtained from intrinsic Pu colloids formed in alkaline solution are much higher than the measured Pu concentrations, suggesting that these three types of intrinsic Pu colloids are more stable, thus less reactive than the ones formed in alkaline solution. The differences in the reactivity among investigated intrinsic Pu colloids are attributed to their morphological features including crystallinity, crystal growth, aggregation and particle shapes and sizes, all of which are greatly influenced by temperatures during formation of these intrinsic Pu colloids. Intrinsic Pu colloids and/or Pu oxides formed at elevated temperatures are more stable and may play an important role in the migration of intrinsic Pu colloids away from

nuclear waste repository setting. Our results suggest that repository scenarios that include higher heat loading may result in stabilization of Pu oxide phases, which can lead to greater migration of intrinsic Pu colloids. However, the repository temperature history, combined with the predicted timing of canister failure and re-saturation of the repository near field will all play a role in the evolution of any specific repository scenario and the potential for Pu mobilization.

Planned FY15 Efforts

Stability of Intrinsic Pu Colloids Across a Range of Repository Conditions

The FY15 effort will build on FY14 experiments summarized in this report. We will extend our current intrinsic Pu colloid stability experimental program to a broader range of geochemical conditions that spans the generic disposal scenarios presently under investigation (salt, argillite, and granite). This work builds on a research program initiated in FY12, where a novel design was developed to study the stability of intrinsic Pu colloids in the presence of montmorillonite clay. In FY14, we completed our study of the stability of intrinsic Pu colloids as a function of temperature and aging in the presence of inorganic colloids at near neutral pH and low salinity groundwater. We determined that the formation conditions of PuO_2 have a dramatic effect on the stability of the colloidal and solid phases in these waters. However, we do not yet know how the wide ranging groundwater conditions in the various repository scenarios may affect the stability of these PuO_2 phases.

In FY15 we will investigate the stability of both low temperature and high fired intrinsic Pu oxides across a wide range of ionic strengths, solution conditions, and temperature that brackets a wider range of repository conditions. Particular focus will be placed on the stabilization of Pu clusters in solution at higher ionic strengths, as observed by Soderholm et al. (2008). Their work suggests that nano-clusters of Pu may be stabilized in high ionic strength solutions due to the specific interaction between PuO_2 clusters and Cl^- counterions. However, the implications to Pu transport in repository environments has not been examined. Stabilization of Pu nano-clusters in higher ionic strength solution could substantially increase Pu mobility in certain repository environments.

Temperature Effects on Bentonite Alteration and Sorption of Actinides

Adsorption and desorption reactions between minerals and radionuclides, which are used to predict their transport in nuclear waste repository scenarios, are routinely performed at temperatures below 303 K.(Begg et al., 2013a; Geckeis et al., 2004; Huber et al., 2011; Sabodina et al., 2006a) However, repository scenarios are likely to involve temperatures at least as high as 360 K.(Cornell, 1993; Rutqvist et al., 2014) There have been a limited number of studies that have demonstrated the importance of temperature on the adsorption of radionuclides such as Cs and Pu.(Long et al., 2013; Lu et al., 2003) Further, previous work has identified that the aqueous complexation U, Np and Pu will change as a function of temperature.(Linfeng et al., 2010) However a systematic study of the effects of temperature on both adsorption and desorption processes of radionuclides and minerals relevant to nuclear waste repository scenarios is lacking. Furthermore, the effect of temperature on mineral alteration and their subsequent sorption behavior has been given very little attention. In FY15, we seek to constrain the effects of temperature on the adsorption/desorption of Pu(IV) and Pu(V) with montmorillonite and its alteration products. This effort will build on our existing experience with Pu and montmorillonite at both ambient and elevated temperatures.(Begg et al., 2013a; Zhao et al., 2012) We will take advantage of the availability of large-volume titanium Parr bomb reactors at LLNL to prepare hydrothermally altered montmorillonite and bentonite rock (6 months alteration at 200ºC). The sorption/desorption of Pu(IV) and Pu(V) to both pristine and hydrothermally altered rock will be investigated as a function of pH (4-10) and temperature (25-80ºC).

Modeling Colloid Facilitated Pu Transport at the Grimsel CFM Facility

Colloid-facilitated transport of actinides in natural systems and the production/stability of pseudo-colloids as a result of bentonite erosion must be quantified for repository performance assessment. Laboratory sorption/desorption models developed in FY13 and FY14 need to be tested in field-scale demonstrations. In FY15, we will test our sorption/desorption kinetic models using the field data available to the UFD program through the CFM international project at the Grimsel facility, Switzerland.

Due to its swelling properties, plasticity, ion exchange, sorption and sealing capability, bentonite is a good candidate for backfill material proposed to be used in nuclear waste repository scenarios.(Guven, 1990) However, one of the concerns with the use of bentonite as a backfill material is that it can form colloidal particles which may enhance the migration of radionuclide species.(Geckeis et al., 2004; Kersting et al., 1999) As a result, radionuclide (including Pu) adsorption to mineral colloids has been the subject of considerable study. In contrast, desorption reactions have been far less well studied. This is problematic because application of thermodynamic equilibrium parameters in field transport models which incorrectly represent desorption processes are likely to be flawed.(Artinger et al., 2002)
Recently, we have developed a numerical model to describe the adsorption and desorption behavior of Pu with montmorillonite (a primary constituent of bentonite) colloids.(Begg et al., In Prep) To further test the assumptions in our approach, we propose to apply this numerical model to data generated in recent Pu-colloid transport experiments performed at the Grimsel Test Site. Comparison of the model and observed behavior will allow us to verify the applicability of our in field-scale conditions or will otherwise highlight areas of weakness in our understanding of Pu adsorption/desorption mechanisms.

Acknowledgments

This work was performed with funding from the Department of Energy, Nuclear Energy Used Fuel Disposition Program, and under the auspices of the U.S. Department of Energy by Lawrence Livermore National Laboratory under Contract DE-AC52-07NA27344.

References

Altmaier, M., Gaona, X., and Fanghaenel, T., 2013. Recent Advances in Aqueous Actinide Chemistry and Thermodynamics. *Chemical Reviews* **113**, 901-943.

Artinger, R., Schuessler, W., Schaefer, T., and Kim, J. I., 2002. A kinetic study of Am(III)/humic colloid interactions. *Environ Sci Technol* **36**, 4358-4363.

Begg, J. D., Zavarin, M., and Kersting, A. B., 2014. Plutonium Desorption from Mineral Surfaces at Environmental Concentrations of Hydrogen Peroxide. *Environ Sci Technol* **48**, 6201-6210.

Begg, J. D., Zavarin, M., Zhao, P., Tumey, S. J., Powell, B., and Kersting, A. B., 2013a. Pu(V) and Pu(IV) sorption to montmorillonite. *Environ Sci Technol* **47**, 5146-5153.

Begg, J. D., Zavarin, M., Zhao, P. H., Tumey, S. J., Powell, B., and Kersting, A. B., 2013b. Pu(V) and Pu(IV) Sorption to Montmorillonite. *Environ Sci Technol* **47**, 5146-5153.

Begg, J. D. C., Zavarin, M., and Kersting, A., In Prep. Desorption of plutonium from montmorillonite: An experimental and modeling study.

Berner, R. A., 1981. Kinetics of Weathering and Diagenesis. In: Lasaga, A. C. and Kirkpatrick, R. J. Eds.), *Kinetics of Geochemical Processes*. BookCrafters, Inc., Chelsea, Michigan

Bertetti, F. P., Pabalan, R. T., and Almendarez, M. G., 1998. Studies on neptunium(V) sorption on quartz, clinoptilolite, montmorillonite, and a-alumina. In: Jenne, E. A. (Ed.), *Adsorption of Metals by Geomedia*. Academic Press, San Diego.

Cleveland, J. M., 1979. The Chemistry of Plutonium. American Nuclear Society, La Grange Park.

Cornell, R. M., 1993. Adsorption of cesium on minerals: A review. *Journal of Radioanalytical and Nuclear Chemistry* **171**, 483-500.

Dai, M. H., Buesseler, K., and Pike, S. M., 2005. Plutonium in groundwater at the 100K-Area of the US DOE Hanford site. *Journal of Contaminant Hydrology* **76**, 167-189.

Efurd, D. W., Runde, W., Banar, J. C., Janecky, D. R., Kaszuba, J. P., Palmer, P. D., Roensch, F. R., and Tait, C. D., 1998. Neptunium and plutonium solubilities in a Yucca Mountain groundwater. *Environ Sci Technol* **32**, 3893-3900.

Farr, J. D., Schulze, R. K., and Neu, M. P., 2004. Surface chemistry of Pu oxides. *Journal of Nuclear Materials* **328**, 124-136.

Geckeis, H., Schafer, T., Hauser, W., Rabung, T., Missana, T., Degueldre, C., Mori, A., Eikenberg, J., Fierz, T., and Alexander, W. R., 2004. Results of the colloid and radionuclide retention experiment (CRR) at the Grimsel Test Site (GTS), Switzerland - impact of reaction kinetics and speciation on radionuclide migration. *Radiochim Acta* **92**, 765-774.

Guven, N., 1990. Longevity of bentonite as buffer material in a nuclear-waste repository. *Engineering Geology* **28**, 233-247.

Haire, R. G., Lloyd, M. H., Beasley, M. L., and Milligan, W. O., 1971. Aging of Hydrous Plutonium Dioxide *JOURNAL OF ELECTRON MICROSCOPY* **20**, 8-16.

Hocsman, A., Di Nezo, S., Charlet, L., and Avena, M., 2006. On the mechanisms of dissolution of montroydite [HgO(s)]: Dependence of the dissolution rate on pH, temperature, and stirring rate. *J Colloid Interf Sci* **297**, 696-704.

Huber, F., Kunze, P., Geckeis, H., and Schafer, T., 2011. Sorption reversibility kinetics in the ternary system radionuclide-bentonite colloids/nanoparticles-granite fracture filling material. *Applied Geochemistry* **26**, 2226-2237.

Kaszuba, J. P. and Runde, W. H., 1999. The aqueous geochemistry of neptunium: Dynamic control of soluble concentrations with applications to nuclear waste disposal. *Environ Sci Technol* **33**, 4427-4433.

Keeney-Kennicutt, W. L. and Morse, J. W., 1985. The redox chemistry of Pu(V)O2+ interaction with common mineral surfaces in dilute solutions and seawater. *Geochimica Et Cosmochimica Acta* **49**, 2577-2588.

Kersting, A. B., 2013. Plutonium Transport in the Environment. *Inorg Chem* **52**, 3533-3546.

Kersting, A. B., Efurd, D. W., Finnegan, D. L., Rokop, D. J., Smith, D. K., and Thompson, J. L., 1999. Migration of plutonium in ground water at the Nevada Test Site. *Nature* **397**, 56-59.

Kersting, A. B., Zavarin, M., Zhao, P., and Dai, Z., 2012. Radionuclide interaction and transport in representative geologic media 2012. Sandia National Laboratory.

Kozai, N., Ohnuko, T., Matsumoto, J., Banba, T., and Ito, Y., 1996. A study of the specific sorption of neptunium(V) on smectite in low pH solution. *Radiochim. Acta* **75**, 149-158.

Kozai, N., Ohnuky, T., and Muraoka, S., 1993. Sorption characteristics of neptunium by sodium-smectite. *J. Nuclear Sci. Tech.* **30**, 1153-1159.

Lasaga, A. C., 1981. Transition State Theory. In: Lasaga, A. C. and Kirkpatrick, R. J. Eds.), *Kinetics of Geochemical Processes*. BookCrafters, Inc., Chelsea, Michigan

Lasaga, A. C., 1998a. *Kinetic Theory in the Earth Sciences*. Princeton University Press, Princeton, NJ.

Lasaga, A. C., 1998b. *Kinetic Theory in the Earth Sciences*. Princeton University Press, Princeton, NJ.

Lasaga, A. C. and Luttge, A., 2004. Mineralogical approaches to fundamental crystal dissolution kinetics. *Am Mineral* **89**, 527-540.

Lemire, R. J., 2001. *Chemical Thermodynamics of Neptunium and Plutonium, Volume 4*. Elsevier Science (September 9, 2001)

Linfeng, R., Guoxin, T., Yuanxian, X., Judah, I. F., PierLuigi, Z., and Plinio Di, B., 2010. Bridging the Gap in the Chemical Thermodynamic Database for Nuclear Waste Repository: Studies of the Effect of Temperature on Actinide Complexation, *Nuclear Energy and the Environment*. American Chemical Society.

Long, H., Wu, P., and Zhu, N., 2013. Evaluation of Cs+ removal from aqueous solution by adsorption on ethylamine-modified montmorillonite. *Chemical Engineering Journal* **225**, 237-244.

Lu, N. P., Reimus, P. W., Parker, G. R., Conca, J. L., and Triay, I. R., 2003. Sorption kinetics and impact of temperature, ionic strength and colloid concentration on the adsorption of plutonium-239 by inorganic colloids. *Radiochim Acta* **91**, 713-720.

Lujaniene, G., Motiejunas, S., and Sapolaite, J., 2007. Sorption of Cs, Pu and Am on clay minerals. *Journal of Radioanalytical and Nuclear Chemistry* **274**, 345-353.

Machuron-Mandard, X. and Madic, C., 1996. Plutonium dioxide particle properties as a function of calcination temperature. *Journal of Alloys and Compounds* **235**, 216-224.

Management, O. o. C. R. W., 2002. Yucca Mountain Science and Engineering Report: Technical Information Supporting Site Recommendation Consideration. U.S. Department of Energy.

Mewhinney, J. A., Rothenberg, S. J., Eidson, A. F., Newton, G. J., and Scripsick, R. C., 1987. Specific Surface-Area Determinations of U and Pu Oxide Particles. *J Colloid Interf Sci* **116**, 555-562.

Neck, V., Altmaier, M., and Fanghaenel, T., 2007a. Thermodynamic data for hydrous and anhydrous PuO2+x(S). *Journal of Alloys and Compounds* **444**, 464-469.

Neck, V., Altmaier, M., and Fanghanel, T., 2007b. Solubility of plutonium hydroxides/hydrous oxides under reducing conditions and in the presence of oxygen. *Cr Chim* **10**, 959-977.

Neck, V., Altmaier, M., Seibert, A., Yun, J. I., Marquardt, C. M., and Fanghanel, T., 2007c. Solubility and redox reactions of Pu(IV) hydrous oxide: Evidence for the formation of PuO2+x(s, hyd). *Radiochimica Acta* **95**, 193-207.

Neck, V., Altmaier, M., Seibert, A., Yun, J. I., Marquardt, C. M., and Fanghanel, T., 2007d. Solubility and redox reactions of Pu(IV) hydrous oxide: Evidence for the formation of PuO(2+x)(s, hyd). *Radiochim Acta* **95**, 193-207.

Neck, V. and Kim, J. I., 2001. Solubility and hydrolysis of tetravalent actinides. *Radiochim Acta* **89**, 1-16.

Nitsche, H., Gatti, R. C., Standifer, E. M., Lee, S. C., Muller, A., Prussin, T., Deinhammer, R. S., Maurer, H., Becraft, K., Leung, S., and Carpenter, S. A., 1993. Measured solubilites and speciations of neptunium, plutonium, and americium in a typical groundwater (J-13) from the Yucca Mountain region. Los Alamos National Laboratory, Los Alamos, NM.

Nitsche, H., Roberts, K., Prussin, T., Muller, A., Becraft, K., Keeney, D., Carpenter, S. A., and Gatti, R. C., 1994. Measured solubilities and speciations from oversaturation experiments of neptunium, plutonium, and americium in UE-25p #1 well from the Yucca Mountain region. Los Alamos National Laboratory, Los Alamos.

Novikov, A. P., Kalmykov, S. N., Utsunomiya, S., Ewing, R. C., Horreard, F., Merkulov, A., Clark, S. B., Tkachev, V. V., and Myasoedov, B. F., 2006. Colloid transport of plutonium in the far-field of the Mayak Production Association, Russia. *Science* **314**, 638-641.

Park, J. F., Catt, D. L., Craig, D. K., Olson, R. J., and Smith, V. H., 1973. Solubility Changes of 238 Pu Oxide in Water Suspension and Effect on Biological Behavior after Inhalation by Beagle Dogs., U.S. Department of Commerce, National Technical Information Service.

Powell, B. A., Fjeld, R. A., Kaplan, D. I., Coates, J. T., and Serkiz, S. M., 2004. Pu(V)O2+ adsorption and reduction by synthetic magnetite (Fe3O4). *Environ Sci Technol* **38**, 6016-6024.

Powell, B. A., Fjeld, R. A., Kaplan, D. I., Coates, J. T., and Serkiz, S. M., 2005. Pu(V)O2+ adsorption and reduction by synthetic hematite and goethite. *Environ Sci Technol* **39**, 2107-2114.

Powell, B. A., Kersting, A. B., and Zavarin, M., 2008. Sorption and Desorption Rates of Neptunium and Plutonium on Goethite. In: Zavarin, M., Kersting, A. B., Lindvall, R. E., and Rose, T. P. Eds.), *Hydrologic Resources Management Program and Underground Test Area Project, FY 2006 Progress Report*. Lawrence Livermore National Laboratory, Livermore, CA.

Rai, D. and Ryan, J. L., 1982. Crystallinity and Solubility of Pu(Iv) Oxide and Hydrous Oxide in Aged Aqueous Suspensions. *Radiochim Acta* **30**, 213-216.

Rao, L. F., Srinivasan, T. G., Garnov, A. Y., Zanonato, P. L., Di Bernardo, P., and Bismondo, A., 2004. Hydrolysis of neptunium(V) at variable temperatures (10-85 degrees C). *Geochimica Et Cosmochimica Acta* **68**, 4821-4830.

Rao, L. F., Tian, G. X., Di Bernardo, P., and Zanonato, P., 2011. Hydrolysis of Plutonium(VI) at Variable Temperatures (283-343 K). *Chem-Eur J* **17**, 10985-10993.

Runde, W., Conradson, S. D., Wes Efurd, D., Lu, N., VanPelt, C. E., and Tait, C. D., 2002. Solubility and sorption of redox-sensitive radionuclides (Np, Pu) in J-13 water from the Yucca Mountain site: comparison between experiment and theory. *Applied Geochemistry* **17**, 837-853.

Rutqvist, J., Zheng, L. G., Chen, F., Liu, H. H., and Birkholzer, J., 2014. Modeling of Coupled Thermo-Hydro-Mechanical Processes with Links to Geochemistry Associated with Bentonite-Backfilled Repository Tunnels in Clay Formations. *Rock Mech. Rock Eng.* **47**, 167-186.

Sabodina, M. N., Kalmykov, S. N., Sapozhnikov, Y. A., and Zakharova, E. V., 2006a. Neptunium, plutonium and ^{137}Cs sorption by bentonite clays and their speciation in pore waters. *Journal of Radioanalytical and Nuclear Chemistry* **270**, 349-355.

Sabodina, M. N., Kalmykov, S. N., Sapozhnikov, Y. A., and Zkharova, E. V., 2006b. Neptunium, plutonium and ^{137}Cs sorption by bentonite clays and their speciation in pore waters. *J. Radioanal. Nucl. Chem.* **270**, 349-355.

Sanchez, A. L., Murray, J. W., and Sibley, T. H., 1985. The adsorption of plutonium IV and V on goethite. *Geochimica Et Cosmochimica Acta* **49**, 2297-2307.

Santschi, P. H., Roberts, K. A., and Guo, L. D., 2002a. Organic mature of colloidal actinides transported in surface water environments. *Environ Sci Technol* **36**, 3711-3719.

Santschi, P. H., Roberts, K. A., and Guo, L. D., 2002b. Organic nature of colloidal actinides transported in surface water environments. *Environ Sci Technol* **36**, 3711-3719.

Stumm, W., 1997. Reactivity at the mineral-water interface: dissolution and inhibition. *Colloids and Surfaces A: Physicochemical and Engineering Aspects* **120**, 143-166.

Turner, D. R., Pabalan, R. T., and Bertetti, F. P., 1998. Neptunium(V) sorption on montmorillonite: An experimental and surface complexation modeling study. *Clays and Clay Minerals* **46**, 256-269.

Walther, C. and Denecke, M. A., 2013. Actinide Colloids and Particles of Environmental Concern. *Chemical Reviews* **113**, 995-1015.

Zhao, P., Kersting, A. B., Dai, Z., and Zavarin, M., 2012. Pu(IV) Intrinsic Colloid Stability in the Presence of Montmorillonite at 25 & 80 C.